Design, Construction, and Validation of a Cadaver Knee Motion Testing Device

Undergraduate Honors Thesis

Presented in Partial Fulfillment of the Requirements for
Graduation with Distinction in the
Department of Mechanical Engineering at
The Ohio State University

by

Julie Ann Thompson

May 2008

Advisor: Robert A. Siston, Ph.D.

Abstract

The knee joint is complex. Surgical procedures such as ACL reconstruction and total knee arthroplasty (TKA) are commonly used to alleviate pain and restore function in knees that suffer from injury or disease. These surgeries affect the kinematics of the joint. It is important to understand exactly how surgical procedures affect knee motion in order to be able to better restore normal joint function post-operatively. Knee kinematics are best investigated in actual knees; however, since it is unethical to simulate surgery in living subjects, there is a need to utilize cadaver specimens. Previous research studies have used various testing devices to study the knee, including robotic systems, weight and pulley systems, and systems involving pneumatic actuators. The limitations of existing devices have motivated the development of a new device. The goal of this project was to design, construct, and validate a cadaver knee motion testing device using passive motion for the purpose of understanding how surgical procedures affect knee kinematics. I used my knowledge of kinematics, machine design, and biomechanics for the design of the mechanism. The construction of the entire device was completed in the Scott Lab student machine shop. The device is controlled through the LabVIEW software using an open-loop control, with the goal of eventually implementing closed-loop control with the use of a potentiometer. The effects of a variety of procedures and surgical parameters on knee motion will be obtained using the device and will be beneficial in motivating possible future improvements in prosthetic design and surgical technique.

Acknowledgements

Many people had a hand in the success of this project. First, I have to thank my advisor, Dr. Rob Siston. My accomplishments over this past year are a result of his constant support, guidance, and encouragement. He has pushed me to work harder than I ever thought I could, and as a result I have done more than I ever imagined I could. There aren't enough pages for me to express how thankful I am for his unwavering faith in my abilities.

I also need to thank Dr. Ajit Chaudhari for his help and advice and for allowing me to look at his CPM machine (in his home, no less) after he had knee surgery. I would also like to thank Dr. Jim Schmiedeler, whose help with my initial kinematic vector loop analysis kept me from losing my mind last summer. A special thanks to Dr. John Bolte as well for showing me his lab and providing me with my first cadaver experiences. Mr. Mark Reep from Breg, Inc. also deserves my thanks for trusting me to keep one of his CPM machines in the lab all summer (and at no charge)!

I owe a huge thank you to Neil Gardner in the Scott Lab student machine shop. He taught me how to use all of the machines in the shop and provided countless tips and advice on the construction of my device. In the span of 3 months I went from having absolutely no machining experience whatsoever to being able to make almost anything out of a block of aluminum. Needless to say, Neil is a very patient and understanding man. It is no exaggeration when I say that the completion of my project wouldn't have been possible without him. I must also thank Gary Gardner for welding many of my parts, which would have been a disaster if I had tried to do it myself. I would also like to thank Caroline Tragni, who sacrificed countless hours of her free time to help me machine some of my parts. She was a huge help and without her I'm sure 3 months of machining would have easily turned into 4 or 5.

A big thank you also goes to my fellow NMBL lab mates, who have provided a lot of advice, suggestions, constructive criticism, and encouragement. Finally, I have to thank my friends and family. Their love and support makes all of the sweat and tears worth it. One of the greatest rewards of this work is the opportunity to make them proud.

Table of Contents

List of Figures

List of Tables

Chapter 1: Introduction

The knee joint is a complex and important part of the human body. Part of its complexity lies in the fact that knee movement involves a set of coupled translations and rotations (Andriacchi et al., 1998). The knee can move in one of two ways. Active motion of the knee joint occurs when the muscles surrounding the knee contract and induce motion. Passive motion involves the movement of the knee joint by an outside force, such as that applied by a doctor or physical therapist.

Figure 1: Anatomy of the knee
www.aclsolutions.com/anatomy

The knee plays an important role in many everyday activities, including walking, running and kneeling, making it vulnerable to a variety of injuries and disorders. Injury to the anterior cruciate ligament (ACL), for example, causes the tibia to slide too far anterior relative to the femur and also affects side-to-side rotation of the lower leg (Figure 2).

Figure 2: Tear of the ACL
www.eorthopod.com

Knee kinematics may also be affected when the joint is diseased (Shiel, 2006), such as by osteoarthritis, which is caused by the breakdown and eventual loss of joint cartilage (Figure 3). Surgical procedures, such as ACL reconstruction and total knee arthroplasty, commonly are required to alleviate pain and restore more normal joint function.

Figure 3: Osteoarthritic joint
www.zimmer.com

In recent years, research has been aimed at discovering how surgical procedures like these affect knee kinematics and what can be done to better restore normal knee motion and function after surgery (Andriacchi et al., 2003, Balasubramanian et al., 2007, Banks et al., 2004, Li et al., 2004, Siston et al., 2006). A thorough understanding of normal knee kinematics is required for achieving this goal. Computer simulations are one method of studying knee kinematics. However, these simulations do not accurately model the full complexity of actual knees (Piazza, 2006). Most simulations model the knee as a single-degree-of-freedom joint with translations and rotations either held fixed or described as a function of flexion angle only (Piazza, 2006). Additionally, accurate contact modeling of the joint surfaces in knee models is computationally intensive (Piazza & Delp, 2001). Measuring joint motion and contact forces in actual knees is ideal. However, since it is unethical to simulate surgery on human subjects, there is a need for an experimental device which can utilize cadaver knee specimens to simulate motion.

Researchers have used a variety of mechanical devices to look into the complex ways in which the knee moves. The work of Wilson et al. (2000), for example, has investigated how knee translation and rotation during passive motion are coupled to flexion angle. The simple testing rig involved holding the tibia fixed on a workbench and flexing and extending the femur by manually rotating a rod inserted in the femur's distal end (Wilson et al., 2000). Li et al. (2004) used a robotic testing system to determine the motion of cadaver knee specimens in response to external loads. The testing apparatus of Balasubramanian et al. (2007) makes use of the action of a force couple to flex and extend the knee specimen through a range of motion of 90 degrees. Simulated muscle loads are applied using a system of weights and pulleys to study the active knee kinematics (Balasubramanian et al., 2007). Another type of load application system for in

vitro testing of the knee joint involves the use of linear and rotary pneumatic actuators to allow for the six degrees of freedom of the joint over a full range of motion (Bach et al., 1994). This apparatus also uses pneumatic actuators to apply simulated muscle forces (Bach et al., 1994). A current commercial product used to produce knee motion is a continuous passive motion (CPM) machine. A CPM machine is a device often used on patients who have undergone knee surgeries, such as total knee arthroplasty or ACL reconstruction. The device passively flexes and extends the knee at slow speeds, which helps to reduce the swelling that may lead to joint stiffness.

There is great utility for these devices, but each has important limitations which have motivated this project. The robotic testing systems, for example, although extremely accurate are also very costly. Other devices, such as the testing apparatus of Wilson et al. (2000) and the commercial CPM machine are only compatible with either a whole leg or a transected leg. A third important limitation of existing devices is their range of testing speeds. Existing CPM machines, for example, are only capable of simulating knee motion at extremely slow speeds: 30 to 150 deg/min. In order to investigate speeds outside of this range, a new device is needed.

1.1 Focus of Thesis

The purpose of this project was to design, construct, and validate a cadaver knee motion testing device using passive motion for the purpose of understanding how surgical procedures affect knee kinematics. I used my knowledge of kinematics, machine design, and biomechanics to create a device capable of moving a cadaver specimen through a range of motion from 0 to 120 degrees and a range of angular velocities from 30 to 750 degrees/minute using passive motion. Both full-leg specimens and transected knee specimens can be tested with this device.

1.2 Significance of Research

Knee surgeries are very common. In 2003, the NIH estimated that over 300,000 total knee arthroplasties (TKA's) were performed in the United States (NIH, 2004), and that number is expected to increase to 3.48 million by the year 2030 (Kurtz et al., 2007). The number of ACL reconstructions performed each year in the United States is estimated at more than 100,000 (Owings et al., 1998). The number of meniscal surgeries is also very high, with approximately 1 million performed every year in the United States alone (MDI, 2003).

It is important to study knee kinematics under passive loads for a number of reasons. One reason is that passive motion is how a surgeon manipulates the leg inside of the operating room. Another reason is that continuous passive motion (CPM) is often used after surgeries such as ACL repair or TKA to reduce the swelling that may lead to joint stiffness (O'Driscoll & Giori, 2000). Passive motion also allows us to investigate the motion of the joint without the influence of large external or muscle forces, making it possible to focus only on the influence of the surgical procedure.

By building a custom passive motion device, we are able to investigate different joint angles and speeds that are not possible with existing CPM machines. There are no studies validating the benefits of the range of motion and speeds used in current rehabilitation protocols after knee surgery. With this custom device, we will be able to investigate the effects on rehabilitation of flexion angles and speeds that are beyond the capabilities of current commercial products. This device is also unique in that it can be used to simulate motion in not only a full cadaver leg, but also a transected knee specimen. Since this device was built entirely in-house and designed to be used with our current equipment and software, we have complete control over the entire experimental system. If we had instead retrofitted an existing device, we would need

to export data from the device's existing motion control system. Designing and constructing our own custom system also provided a significant cost savings over purchasing and modifying an existing system.

1.3 Overview of Thesis

This thesis has 5 chapters. Chapter 2 discusses the design process for the device. This consists of the mathematical design, including kinematic vector loop equations for determining position and speed, as well as the static force analysis. The chapter also discusses how fundamental machine design concepts were used to select hardware and electronic components. Chapter 3 discusses the mechanics of the design. This includes a detailed description of how the cadaver specimen attaches to the apparatus, the various design changes that I made to reach the final design, and the machining and construction of the device. Chapter 4 discusses the control aspect of the device. This includes a description of the LabVIEW program and motor which are used to control the motion of the testing apparatus. Chapter 5, the conclusion, summarizes the key contributions of this thesis, discusses additional applications of this work, and proposes possible future directions of study.

Chapter 2: Mechanism Design

For my initial design concepts, I focused on crank-rockers and slider-rockers; simple 4-bar mechanisms whose repetitive motion when actuated can be easily translated into a flexion and extension motion of the leg. Another design I considered was that of a continuous passive motion (CPM) machine. I chose the CPM design and a few of my other design ideas to investigate further by creating cardboard prototypes (Figures 4-6).

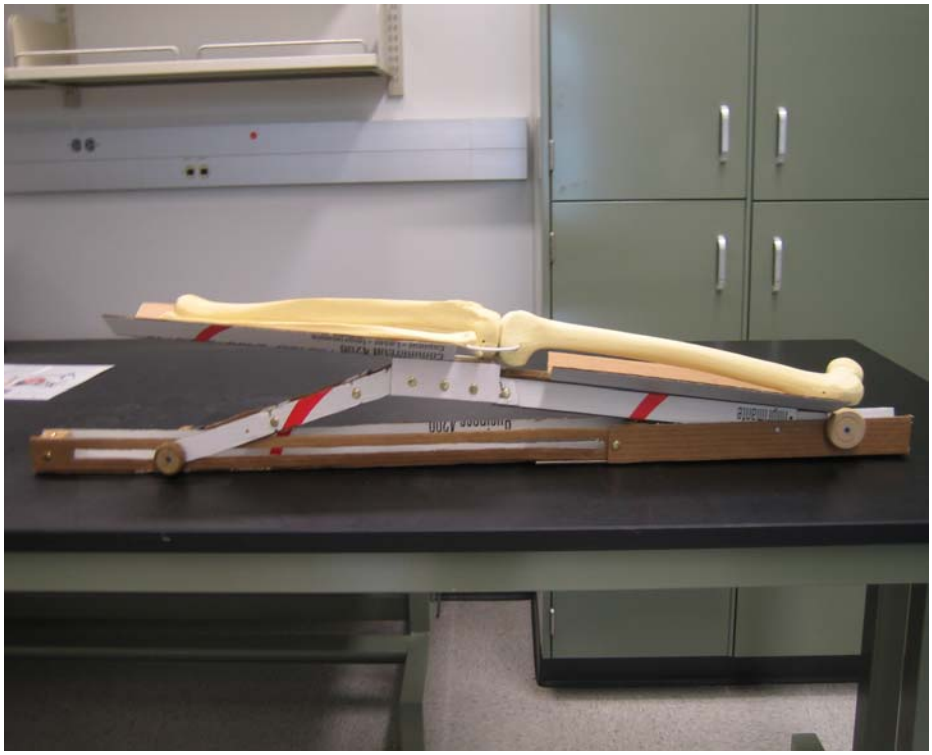

Figure 4: Slider-rocker prototype in full extension
Sawbones of the femur, tibia, and fibula represent the approximate location of the cadaver specimen. The slider joint is located below the distal end of the tibia and just above the surface of the table.

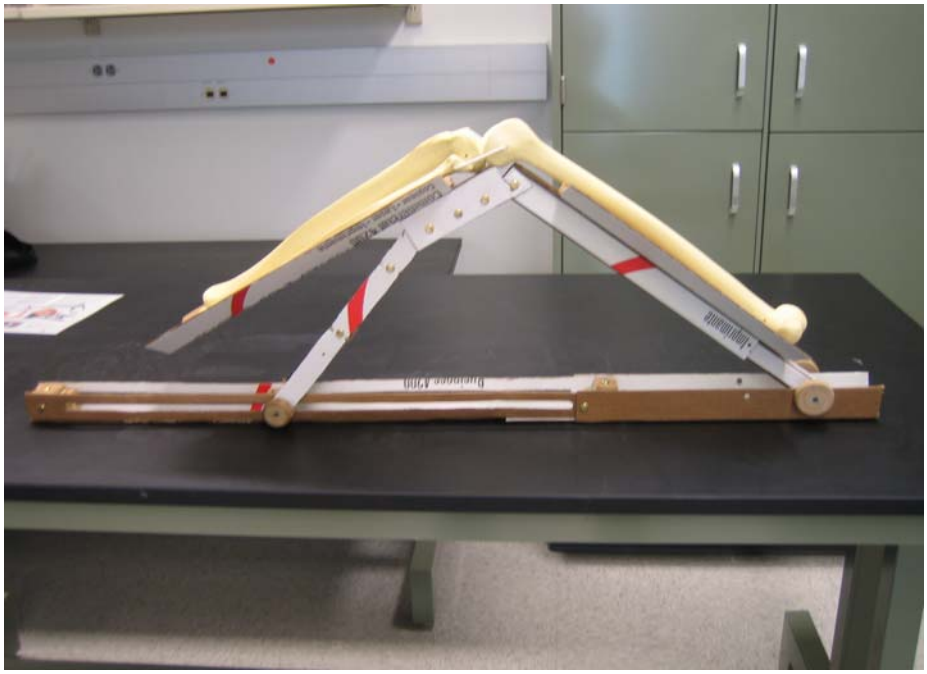

Figure 5: Slider-rocker prototype in flexion
The knee joint of the sawbones is located directly above the center revolute joint of the slider-rocker. The link directly below the femur is able to telescope to different lengths.

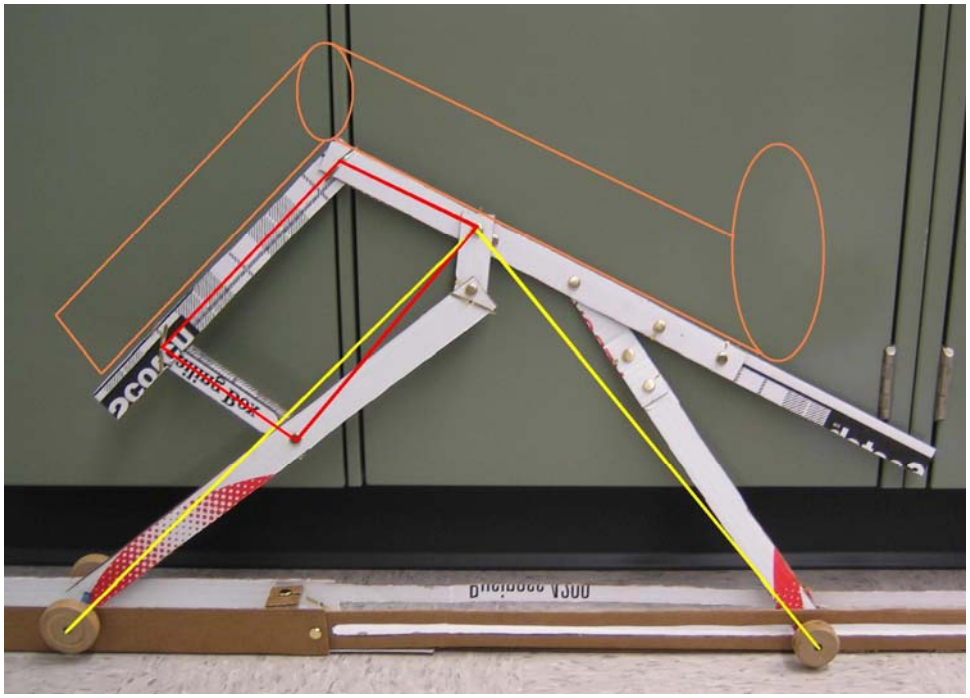

Figure 6: CPM machine prototype
The prototype represents the basic structure of a CPM machine, which is a combination of a slider-rocker (yellow) and 4-bar linkage (red). The 4-bar linkage allows the knee joint to be offset from the center revolute joint of the slider-rocker.

The main advantage of the first prototype is its simplicity (Figures 4-5). The knee joint lies directly over the center joint of the slider-rocker, providing a knee flexion angle that is exactly the same as the angle of the slider-rocker. However, this design lacks stability, most likely due to its narrow base. Additionally, the base of the structure supporting the tibia interferes with the horizontal slider track at high flexion angles. A disadvantage of the CPM design is that it is more complex than a simple slider-rocker. In fact, the design is a combination of a slider-rocker and a 4-bar linkage (Figure 6). The 4-bar linkage allows the knee joint to be offset slightly from the center joint of the slider-rocker. This offset offers a significant advantage over the slider-rocker design by eliminating the interference problem of the first prototype, providing more freedom to adjust the lengths of the links in the device. After analyzing the advantages and disadvantages of each prototype, it became obvious that the best design to use

would be the one based on the CPM machine. To better understand how a CPM works and moves, I was able to find a local company called Breg, Inc. to let me borrow one for the summer (Figure 7).

Figure 7: Commercial CPM machine
The patient's leg rests in the black padding which spans the blue tubing support structure. The speed and flexion angles of the device are controlled with the handheld remote.

By using the CPM as a reference, I determined what the approximate lengths and sizing of the links in the device needed to be. I used anthropometric data (Winter, 2005) to determine the link sizes necessary for my device to accommodate a range of leg lengths (Table 1). Based on this data, I incorporated adjustable telescoping links into the design.

Table 1: Anthropometric segment length data

	Foot length = 0.055*H (in)	Shank length = 0.246*H (in)	Thigh length = 0.245*H (in)
Minimum (H=total height=54")	2.97	13.284	13.23
Average (H=67.3")	3.703	16.5614	16.494
Maximum (H=78")	4.29	19.188	19.11

With the basic size and structure of the design established, I created solid models and drawings of each link in Solid Edge. To ensure that the mechanism would assemble and move correctly, I created a solid model assembly of all parts (Figure 8).

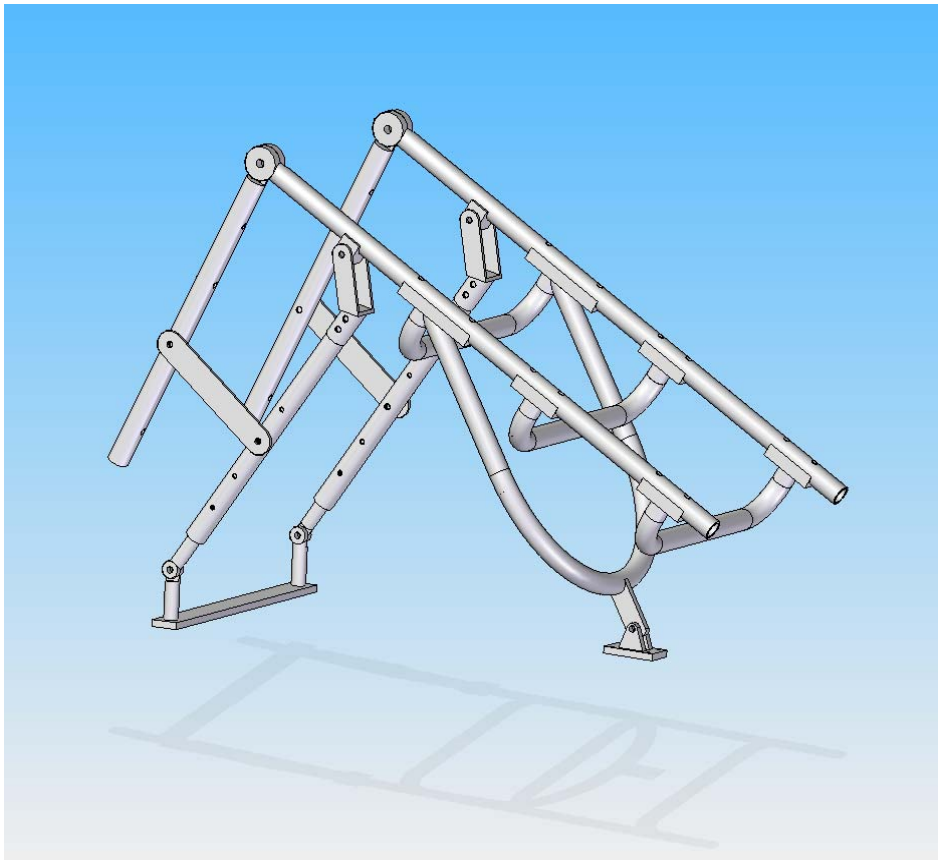

Figure 8: Initial solid model
The majority of the device's structure is composed of round tubing. The base at the lower left of the mechanism is stationary while the slider at the lower right of the mechanism is able to translate back and forth.

The range of motion and angular velocities at the knee joint I have chosen to investigate with my device are based on the specifications of the borrowed CPM machine, with a few important exceptions. The range of angular velocities of which the CPM machine is capable is 30 to 150 degrees per minute (Table 2). However, there is little research explaining why this is the accepted range. In order to investigate the effect of moving the knee at speeds outside of this range, I chose to design my custom CPM device with a range of 30 to 750 degrees per minute. In addition, the existing CPM machine has a range of motion which is only adjustable in 10 degree increments. My device has an angular control of less than 2 degrees, so the flexion angle at the knee joint can be specified anywhere between 0 and 120 degrees of flexion in 2 degree increments.

Table 2: Existing CPM specifications compared to custom CPM specifications

	Range of Motion (degrees)	Range of Motion Adjustability (degrees)	Angular Velocity at Knee Joint (degrees/minute)
Commercial CPM	-10 to 120	10	30 to 150
Custom CPM	0 to 120	2	30 to 750

From here, it was necessary to determine what forces, travel distances, and speeds are required at the slider component to obtain the desired flexion angles and angular velocities at the knee joint. This analysis proved to be challenging because the design is a combination of a kinematic slider-rocker and a 4-bar double rocker linkage. To solve these problems, I used kinematic vector loop equations to determine the slider position and speed at any given knee flexion angle and angular velocity. The variables in the vector loop equations are based on the angles and lengths of each link in the slider-rocker and 4-bar linkages (Figure 9).

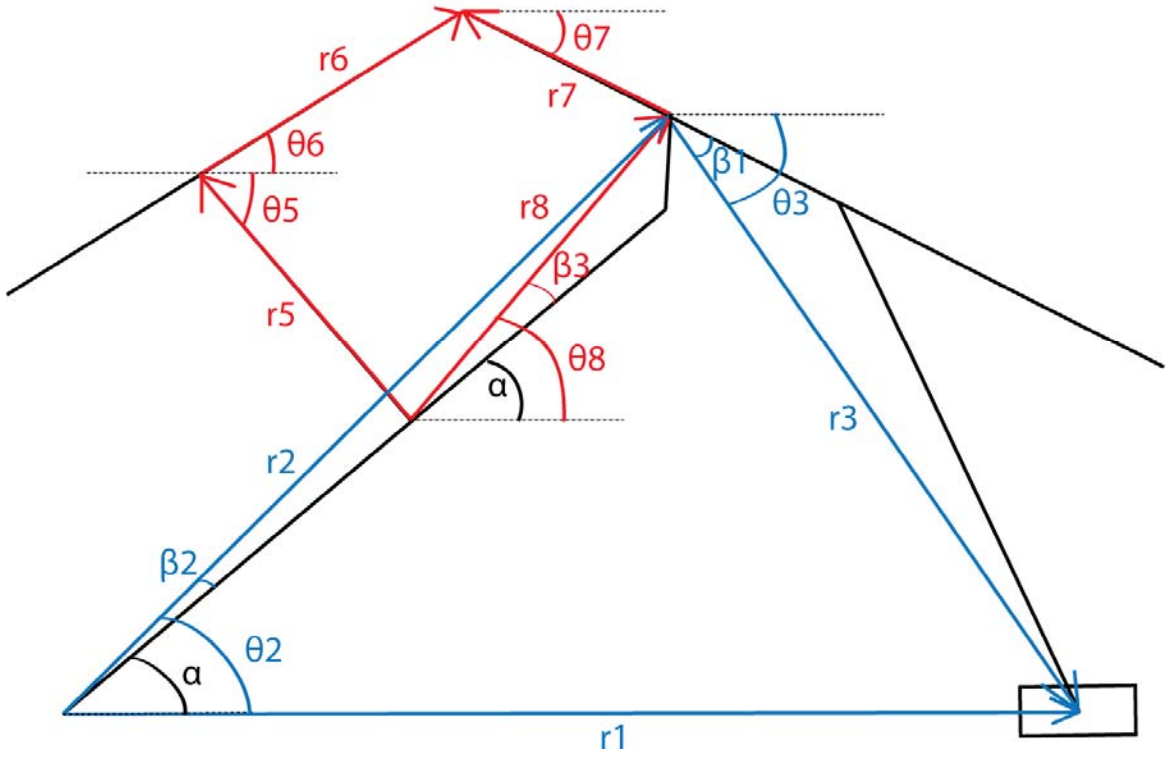

Figure 9: Lengths and angles of device links
The slider-rocker is outlined in blue and the 4-bar mechanism is outlined in red.

For an average leg length of 36.76” and knee flexion angle of 45 degrees, for example, vector loop equations (Waldron & Kinzel, 2004) can provide the relationship between the position and speed of the slider and the flexion angle and angular velocity at the knee.

For the slider-rocker, the known quantities are:

$r_1 = 27.589"$

$r_{telescope} = 15.5"$

$$r_2 = \sqrt{r_{telescope}{}^2 + 2.125^2 - 2r_{telescope} * 2.125\cos\left(\frac{135*\pi}{180}\right)} = 17.0689"$$

$r_3 = 16.461"$

$r_4 = 0$

$\theta_1 = 0$

$\theta_4 = 0$

$$\beta_1 = \cos^{-1}\left(\frac{{r_2}^2 + {r_{telescope}}^2 - 2.125^2}{2r_2 r_{telescope}}\right)\left(\frac{180}{\pi}\right)$$

$$= \cos^{-1}\left(\frac{(17.0689)^2 + (15.5)^2 - 2.125^2}{2(17.0689)(15.5)}\right)\left(\frac{180}{\pi}\right)$$

$$= 5.0504^o$$

The general forms of the equations for the slider-rocker are then:

$$r_{slider} = r_1 = r_2 + r_3$$

$$r_3 \cos\theta_3 = r_1 \cos\theta_1 - r_2 \cos\theta_2$$

$$r_3 \sin\theta_3 = r_1 \sin\theta_1 - r_2 \sin\theta_2$$

$${r_3}^2 = {r_1}^2 + {r_2}^2 - 2r_1 r_2 \left(\cos\theta_1 \cos\theta_2 + \sin\theta_1 \sin\theta_2\right)$$

$$A\cos\theta_2 + B\sin\theta_2 + C = 0$$

$$A = -2r_1 r_2 \cos\theta_1$$

$$B = -2r_1 r_2 \sin\theta_1$$

$$C = {r_1}^2 + {r_2}^2 - {r_3}^2$$

Simplifying with trigonometric identities gives:

$$A(1-t^2) + B(2t) + C(1+t^2) = 0$$

$$t = \tan\left(\frac{\theta_2}{2}\right)$$

$$t = \frac{-B \pm \sqrt{B^2 - C^2 + A^2}}{C - A}$$

$$\theta_2 = 2\tan^{-1} t$$

$$\theta_3 = \tan^{-1}\left[\frac{r_1 \sin\theta_1 + r_4 \sin\theta_4 - r_2 \sin\theta_2}{r_1 \cos\theta_1 + r_4 \cos\theta_4 - r_2 \cos\theta_2}\right]$$

Plugging the known quantities into these general equations gives:

$$\mathrm{A} = -2(27.589)(17.0689)\cos(0)$$

$$= -941.826$$

$$B = -2(27.589)(17.0689)\sin(0)$$

$$= 0$$

$$C = (27.589)^2 + (17.0689)^2 - (16.461)^2$$

$$= 781.5347$$

$$\mathrm{t} = \frac{-0 \pm \sqrt{0^2 - 781.5347^2 + (-941.826)^2}}{781.5347 - (-941.826)}$$

$$= 0.305 \quad \text{(assembly mode +1)}$$

$$\theta_2 = 2\tan^{-1}(0.305)$$
$$= 0.592 \text{ radians}$$
$$\theta_{2,\text{degrees}} = \text{atan2}(\sin(0.592),\cos(0.592))\left(\frac{180}{\pi}\right)$$
$$= 33.921^o$$
$$\theta_3 = \tan^{-1}\left[\frac{27.589\sin(0)+(0)\sin(0)-17.0689\sin(0.592)}{27.589\cos(0)+(0)\cos(0)-17.0689\cos(0.592)}\right]$$
$$= -0.6171 \text{ radians}$$
$$\theta_{3,\text{degrees}} = \text{atan2}(\sin(-0.6171),\cos(-0.6171))\left(\frac{180}{\pi}\right)$$
$$= -35.3561^o$$

Similarly, for the 4-bar mechanism, the known quantities are:

$r_5 = 4.875"$

$r_6 = 7.6875"$

$r_7 = 4.5625"$

$r_8 = 8.45"$

$$\theta_7 = \theta_{3,\text{degrees}} + 23.0214^0$$
$$= -35.3561^o + 23.0214^o$$
$$= -12.3347^o$$
$$\theta_8 = \theta_{2,\text{degrees}} + 10.241^0 - \beta_1$$
$$= 33.921^o + 10.241^o - 5.0504^o$$
$$= 39.1116^o$$

The general forms of the equations for the 4-bar mechanism are:

$$r_5 + r_6 = r_8 + r_7$$
$$A = 2r_7 r_6 \cos\theta_7 - 2r_8 r_6 \cos\theta_8$$
$$B = 2r_7 r_6 \sin\theta_7 - 2r_8 r_6 \sin\theta_8$$
$$C = r_7^{\,2} + r_8^{\,2} + r_6^{\,2} - r_5^{\,2} - 2r_7 r_8\left(\cos\theta_7\cos\theta_8 + \sin\theta_7\sin\theta_8\right)$$
$$t = \frac{-B \pm \sqrt{B^2 - C^2 + A^2}}{C - A}$$
$$\theta_6 = 2\tan^{-1} t$$
$$\theta_5 = \tan^{-1}\left[\frac{r_7\sin\theta_7 + r_6\sin\theta_6 - r_8\sin\theta_8}{r_7\cos\theta_7 + r_6\cos\theta_6 - r_8\cos\theta_8}\right]$$

Plugging the known quantities into these equations gives:

$$A = 2(4.5625)(7.6875)\cos(-12.3347) - 2(8.45)(7.6875)\cos(39.1116)$$
$$= -32.2772$$
$$B = 2(4.5625)(7.6875)\sin(-12.3347) - 2(8.45)(7.6875)\sin(39.1116)$$
$$= -96.9423$$
$$C = (4.5625)^2 + (8.45)^2 + (7.6875)^2 - (4.875)^2$$
$$- 2(4.5625)(8.45)(\cos(-12.3347)\cos(39.1116) + \sin(-12.3347)\sin(39.1116))$$
$$= 79.4947$$
$$t = \frac{-(-96.9423) \pm \sqrt{(-96.9423)^2 - (79.4947)^2 + (-32.2772)^2}}{79.4947 - (-32.2772)}$$
$$= 0.2930 \quad \text{(assembly mode -1)}$$
$$\theta_6 = 2\tan^{-1}(0.2930)$$
$$= 0.5701 \text{ radians}$$
$$\theta_{6,\text{degrees}} = \text{atan2}(\sin(0.5701), \cos(0.5701))\left(\frac{180}{\pi}\right)$$
$$= 32.6651^o$$
$$\theta_5 = \tan^{-1}\left[\frac{4.5625\sin(-12.3347) + 7.6875\sin(32.6651) - 8.45\sin(39.1116)}{4.5625\cos(-12.3347) + 7.6875\cos(32.6651) - 8.45\cos(39.1116)}\right]$$
$$= -0.4581 \text{ radians}$$
$$\theta_{5,\text{degrees}} = \text{atan2}(\sin(-0.4581), \cos(-0.4581))\left(\frac{180}{\pi}\right)$$
$$= -26.2484^o$$

The knee flexion angle can then be solved using the following equation:

$$Knee_{\text{flexion angle}} = 180^0 - \alpha$$

where $\alpha = \theta_7 - \theta_{6,\text{degrees}} + 180^0$

$$= -12.3347^o - 32.6651^o + 180^o$$
$$= 135.0002^o$$

Therefore, the knee flexion angle is: $Knee_{\text{flexion angle}} = 180^o - 135.0002^o$

$$= 45^o$$

For an average leg length of 36.76” and flexion angle of 45 degrees, as well as an angular velocity of 150 deg/min, the following calculations provide the relationship between the velocity of the slider and angular velocity at the knee:

$$\dot{r}_1 = 21.375 \text{ in/min}$$

$$\begin{bmatrix} -r_2 \sin\theta_2 & -r_3 \sin\theta_3 \\ r_2 \cos\theta_2 & r_3 \cos\theta_3 \end{bmatrix} \begin{bmatrix} \dot{\theta}_2 \\ \dot{\theta}_3 \end{bmatrix} = \begin{bmatrix} \dot{r}_1 \\ 0 \end{bmatrix}$$

$$\begin{bmatrix} -17.0689\sin(0.592) & -16.461\sin(-0.6171) \\ 17.0689\cos(0.592) & 16.461\cos(-0.6171) \end{bmatrix} \begin{bmatrix} \dot{\theta}_2 \\ \dot{\theta}_3 \end{bmatrix} = \begin{bmatrix} 21.375 \\ 0 \end{bmatrix}$$

$$\dot{\theta}_2 = -62.5653 \text{ deg/min}$$

$$\dot{\theta}_3 = 66.0082 \text{ deg/min}$$

$$\dot{\theta}_7 = \dot{\theta}_3 = 66.0082 \text{ deg/min}$$

$$\dot{\theta}_8 = \dot{\theta}_2 = -62.5653 \text{ deg/min}$$

$$\begin{bmatrix} -r_5 \sin\theta_5 & r_6 \sin\theta_6 \\ -r_5 \cos\theta_5 & r_6 \cos\theta_6 \end{bmatrix} \begin{bmatrix} \dot{\theta}_5 \\ \dot{\theta}_6 \end{bmatrix} = \begin{bmatrix} r_8\dot{\theta}_8 \sin\theta_8 - r_7\dot{\theta}_7 \sin\theta_7 \\ r_8\dot{\theta}_8 \cos\theta_8 - r_7\dot{\theta}_7 \cos\theta_7 \end{bmatrix}$$

$$\begin{bmatrix} -4.875\sin(-26.2484^o) & 7.6875\sin(32.6651^o) \\ -4.875\cos(-26.2484^o) & 7.6875\cos(32.6651^o) \end{bmatrix} \begin{bmatrix} \dot{\theta}_5 \\ \dot{\theta}_6 \end{bmatrix} =$$

$$\begin{bmatrix} (8.45)(-62.5653)\sin(39.1116^o) - (4.5625)(66.0082)\sin(-12.3347^o) \\ (8.45)(-62.5653)\cos(39.1116^o) - (4.5625)(66.0082)\cos(-12.3347^o) \end{bmatrix}$$

$$\dot{\theta}_5 = 36.7902^o$$

$$\dot{\theta}_6 = -83.9914^o$$

$$Knee_{\text{flexion speed}} = \dot{\theta}_7 - \dot{\theta}_6$$

$$= 66.0082 \text{ deg/min - (-83.9914 deg/min)}$$

$$= 150 \text{ deg/min}$$

I determined the horizontal force required at the slider to hold the testing frame in any given position by performing a simple static force analysis. I again used anthropometric data (Winter, 2005) to determine the maximum mass expected for each segment of the leg: foot, shank, and thigh (Table 3). I assumed a maximum total subject mass of 225 lbs. This data was then used to calculate the force exerted by each leg segment on the device.

Table 3: Anthropometric mass data

Foot mass = 0.0145*M (M=total mass=225 lbs) lbs (Newtons)	Shank mass = 0.0465*M lbs (Newtons)	Thigh mass = 0.1*M lbs (Newtons)
3.2625 (14.512)	10.4625 (46.54)	22.5 (100.085)

The force of each segment was assumed to act at its respective center of mass. I approximated the center of mass for each segment according to anthropometric data (Table 4) (Winter, 2005).

Table 4: Center of mass positions

	Foot COM = 0.5*L (in) from ankle (L=segment length)	Foot COM (in) from knee	Shank COM = 0.433*L (in) from knee	Thigh COM = 0.433*L (in) from hip	Thigh COM = 0.567*L (in) from knee
Minimum	1.485	14.769	5.752	5.729	7.501
Average	1.8514	18.413	7.171	7.142	9.352
Maximum	2.145	21.333	8.308	8.275	10.835

Force Equations:

$$F_{thigh} = 100.085 \text{ N}$$
$$F_{shank} = 46.54 \text{ N}$$
$$F_{foot} = 14.512 \text{ N}$$

using values for average leg length (Table 4):

$$com_{thigh} = 9.352"$$
$$com_{shank} = 7.171"$$
$$com_{foot} = 18.413"$$

$$F_{43,y} = \frac{-F_{thigh} * com_{thigh} * \cos\theta_6}{\frac{r_5 \cos|\theta_5| * r_6 \sin\theta_6}{r_5 \sin|\theta_5|} + r_6 \cos\theta_6}$$

$$= \frac{-(100.085N)(9.352") \cos(0.5701)}{\frac{(4.875") \cos|-0.4581| * (7.6875") \sin(0.5701)}{(4.875") \sin|-0.4581|} + (7.6875") \cos(0.5701)}$$

$$= -52.9333 \text{ N}$$

$$F_{43,x} = \frac{-F_{43,y} * r_5 \cos|\theta_5|}{r_5 \sin|\theta_5|}$$

$$= \frac{-(-52.9333N)(4.875") \cos|-0.4581|}{(4.875") \sin|-0.4581|}$$

$$= 107.3454 \text{ N}$$

$$F_{54,y} = F_{thigh} + F_{43,y}$$

$$= 100.085N + (-52.9333N)$$

$$= 47.1517 \text{ N}$$

$$F_{54,x} = F_{43,x} = 107.3454 \text{ N}$$

$$F_{32,y} = F_{43,y} = -52.9333 \text{ N}$$

$$F_{32,x} = F_{43,x} = 107.3454 \text{ N}$$

$$r_9 = r_{telescope} = 15.5"$$

$$r_{10} = r_9 - 6.8125$$

$$= 15.5" - 6.8125"$$

$$= 8.6875"$$

$$\beta_2 = 6.979^0$$

$$\alpha_2 = 90^0 - \beta_2 - |\theta_{3,\text{degrees}}|$$

$$= 90^o - 6.979^o - |-35.3561^o|$$

$$= 47.6649^o$$

$$a = 12.875 \sin(\alpha_2)$$

$$= 12.875 \sin(47.6649^o)$$

$$= 9.5174"$$

$$b = \frac{a}{\cos|\theta_7|}$$
$$= \frac{9.5174"}{\cos|-12.3347^o|}$$
$$= 9.7423"$$

$$c = com_{foot} - 8.5625 - b$$
$$= 18.413" - 8.5625" - 9.7423"$$
$$= 0.1082"$$

$$d = c * \cos|\theta_7|$$
$$= (0.1082")\cos|-12.3347^o|$$
$$= 0.1057"$$

$$e = (8.5625 - com_{shank}) * \cos|\theta_7|$$
$$= (8.5625" - 7.171")\cos|-12.3347^o|$$
$$= 1.3594"$$

$$f = e + a$$
$$= 1.3594" + 9.5174"$$
$$= 10.8768"$$

$$g = (90^0 - \alpha_2 - 11.915) * \left(\frac{\pi}{180}\right)$$
$$= (90^o - 47.6649^o - 11.915^o)\left(\frac{\pi}{180}\right)$$
$$= 0.5309 \text{ radians}$$

$$\beta_4 = (\theta_2 - 5.089) * \left(\frac{\pi}{180}\right)$$
$$= (33.9210^o - 5.089^o)\left(\frac{\pi}{180}\right)$$
$$= 0.5032 \text{ radians}$$

$$\beta_5 = \beta_4 + \left(\frac{45^* \pi}{180}\right)$$
$$= 0.5032 + \left(\frac{45^o * \pi}{180}\right)$$
$$= 1.2886 \text{ radians}$$

$$h = \frac{r_{10}\left(F_{32,y}\cos\beta_4 - F_{32,x}\sin\beta_4\right)}{r_9\cos\beta_4 + 2.125\cos\beta_5}$$
$$= \frac{(8.6875")((-52.9333N)\cos(0.5032) - (107.3454N)\sin(0.5032))}{(15.5")\cos(0.5032) + 2.125\cos(1.2886)}$$
$$= -60.1663 \text{ N}$$

$$i = -F_{foot}d + F_{shank}f - 16.461^* h\cos|\theta_3| + 20.737\left(F_{54,y}\cos g + F_{54,x}\sin g\right)$$
$$= -(14.512N)(0.1057") + (46.54N)(10.8768") - (16.461")(-60.1663N)\cos|-0.6171|$$
$$+ (20.737")((47.1517N)\cos(0.5309) + (107.3454N)\sin(0.5309))$$
$$= 3.2827^*10^3 \text{ in-N}$$

$$j = \frac{16.461\left(\sin|\theta_3| + \cos|\theta_3|\right)\left(r_9\sin\beta_4 + 2.125\sin\beta_5\right)}{r_9\cos\beta_4 + 2.125\cos\beta_5}$$
$$= \frac{(16.461")(\sin|-0.6171| + \cos|-0.6171|)((15.5")\sin(0.5032) + (2.125")\sin(1.2886))}{(15.5")\cos(0.5032) + (2.125")\cos(1.2886)}$$
$$= 18.5406"$$

$$F_{52,x} = \frac{i}{j} = \frac{3.2827^*10^3 \text{ in-N}}{18.5406"} = 177.0554 \text{ N}$$

$$F_{65,x} = F_{52,x} - F_{54,x} = 177.0554N - 107.3454N = 69.7099 \text{ N}$$
$$F_{slider} = F_{65,x} = 69.7099 \text{ N}$$

I then created a custom MATLAB program which I could use to solve the vector loop equations and force analysis equations. Using this program, I generated plots of slider position, force, and velocity as a function of knee flexion angle (Figures 10-13, average leg length of 36.76”). Using the plot of slider position, we can easily determine the distance of the slider from

the telescoping joint required to obtain a given knee flexion angle in the cadaver specimen. Slider distance decreases as knee flexion angle increases (Figure 10). Similarly, the plot of the static force analysis provides information on the horizontal force required at the slider to hold the mechanism in a given knee flexion angle, assuming a maximum subject mass of 225 lbs (corresponding to a leg mass of 36.225 lbs). The force increases as knee flexion angle increases up to approximately 18 degrees and decreases as flexion angle increases past 18 degrees (Figure 11). The velocity plots illustrate the relationship between the slider velocity and knee flexion angle for any given angular velocity at the knee joint. The horizontal velocity of the slider must increase as knee flexion angle increases in order to keep the angular velocity at the knee constant (Figures 12-13). The velocity profiles of the experimental angular velocities to be investigated with our custom CPM machine are plotted separately from the velocity profiles of current CPM machines (Figure 13). The data in these plots depend of the length of the telescoping links, which are adjustable for a minimum leg length of 29.48 inches, an average leg length of 36.76 inches, and a maximum leg length of 42.59 inches. The plots corresponding to minimum and maximum leg lengths are included in the Appendix as well as all program code.

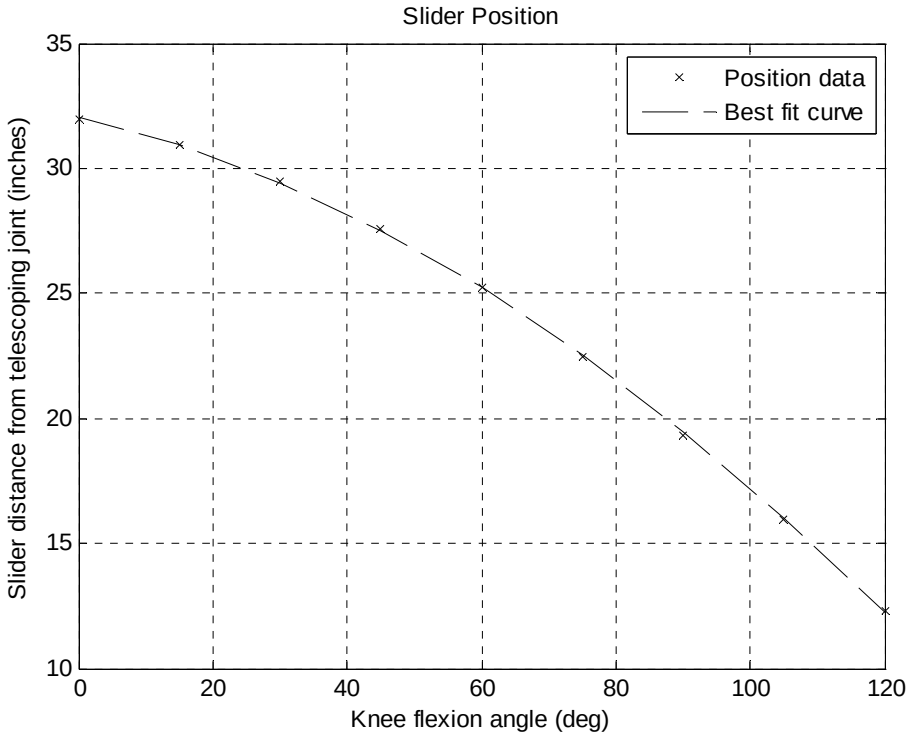

Figure 10: Plot of slider position vs. knee flexion angle

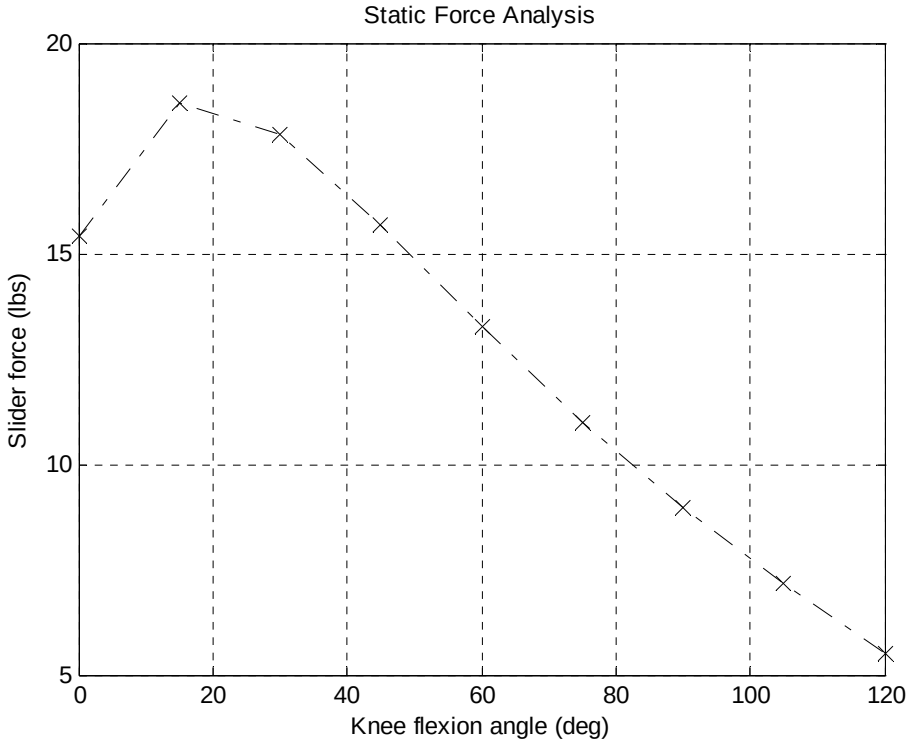

Figure 11: Plot of horizontal slider force vs. knee flexion angle

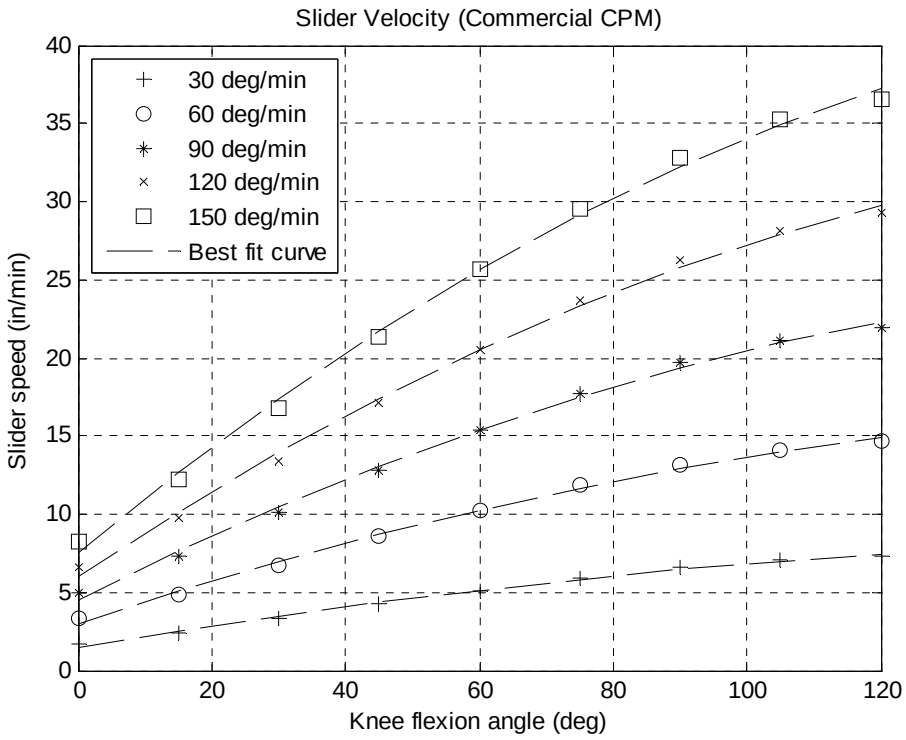

Figure 12: Plot of commercial CPM slider velocities vs. knee flexion angle

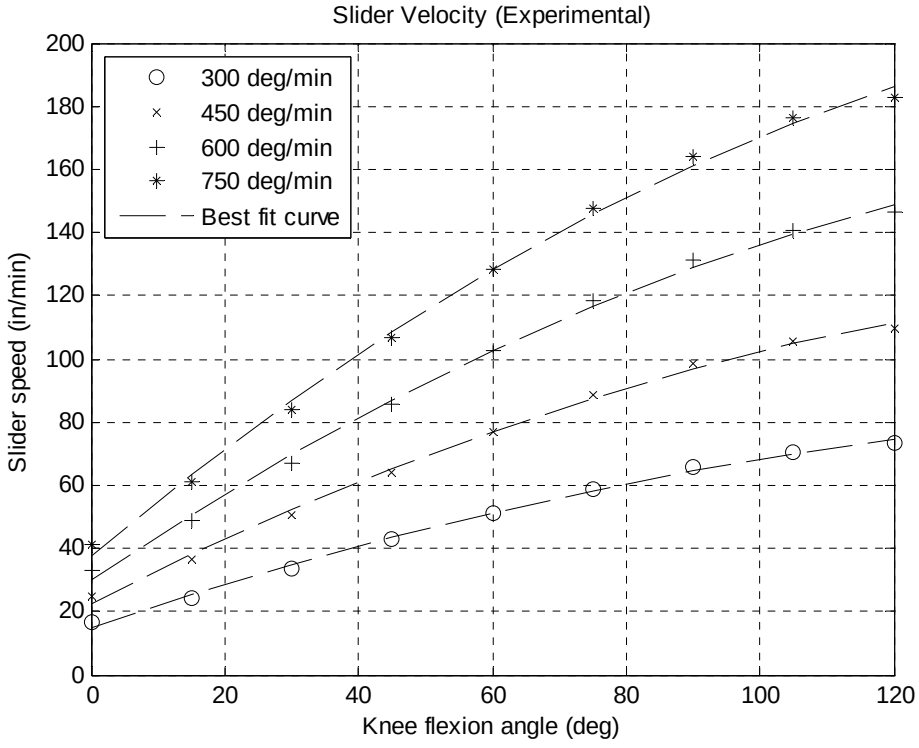

Figure 13: Plot of experimental slider velocities vs. knee flexion angle

To determine the hardware components necessary for my design, I used machine design concepts. I initially selected a lead screw to obtain the linear motion at the sliding joint. Based on the results of my speed and force analyses, I was able to calculate the required diameter, length, material, and other characteristics of the lead screw and nut assembly using basic machine design equations (Collins, 2003) shown below.

Assuming $l = p = 0.2"$, $W = 25$ lb, $\theta = 14.5^o$ and a 3/8" steel screw with a plastic nut,

the torque required for the lead screw is:

$$T_R = Wr_p\left[\frac{l\cos\theta + 2\pi r_p\mu_t}{2\pi r_p\cos\theta - l\mu_t}\right] + Wr_c\mu_c$$

with

$$\mu_t = 0.17$$

$$d_r = d_o - 2\left(\frac{p}{2}\right)$$

$$d_r = \frac{3}{8} - 2\left(\frac{0.2}{2}\right) = 0.175"$$

$$r_p = \frac{p}{4} + r_r = \frac{p}{4} + \frac{d_r}{2}$$

$$r_p = \frac{0.2}{4} + \frac{0.175}{2} = 0.1375"$$

So the torque calculation is as follows:

$$T_R = (25\text{ lb})(0.1375\text{ in})\left[\frac{0.2\cos(14.5) + 2\pi(0.1375)(0.17)}{2\pi(0.1375)\cos(14.5) - (0.2)(0.17)}\right] = 1.459\text{ in-lb}$$

While researching hardware companies, however, I discovered another type of linear motion device called a linear slide (Figure 14).

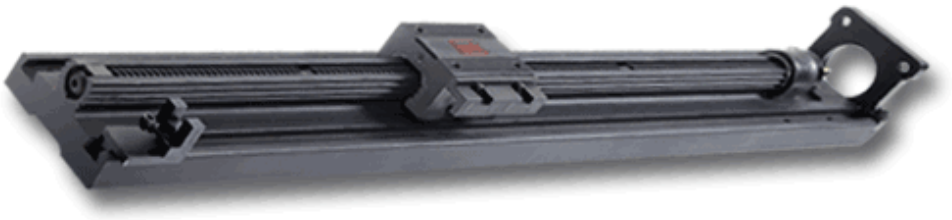

Figure 14: Linear slide
www.kerkmotion.com

Ultimately, I decided to use a linear slide for my motion requirements because of some of the advantages it offers over a simple lead screw and nut assembly. The linear slide provides greater stability, easier mounting for the sliding joint of my device, and is not limited by critical screw speed, meaning that the slide platform which travels along the screw is capable of a higher maximum velocity. This is especially important for my design since I have chosen to investigate velocities higher than what existing CPM machines are capable of achieving. In order to achieve the linear velocities of the slider calculated with the MATLAB program (Figures 12-13), the rotational speed of the screw must be calculated as follows:

$$n = \frac{V}{l}$$

$V =$ linear slider velocity

$l =$ screw lead

The maximum linear velocity calculated with the MATLAB program is

$$\text{slider speed}_{\max} = 190.63 \ \frac{\text{in}}{\text{min}}$$

Therefore, $n = \dfrac{190.63 \ \frac{\text{in}}{\text{min}}}{0.2 \ \frac{\text{in}}{\text{rev}}} = 953.15 \text{ rpm}$

If, for example, we wanted to move the leg from 0 degrees of flexion to 120 degrees of flexion at this speed, then the duration of the move is calculated as follows:

$$(\text{position at } 0^{o} - \text{ position at } 120^{o}) * \frac{1\text{min}}{190.63"}$$

where position at 0 degrees = 34.418” (from MATLAB analysis)
position at 120 degrees = 13.734”

$$(34.418"\text{-}13.734") * \frac{1\text{min}}{190.63"} = 0.1085\,\text{min} = 6.51 \text{ seconds}$$

These speed and time values can then be used as input to a motor, providing open loop control of the device.

Chapter 3: Design Modifications and Construction

The initial mechanism design underwent numerous changes and modifications to reach the final design. One of the earliest changes was an increase in the link lengths on either side of the cadaver specimen. This adjustment will enable the device to accommodate a greater range of cadaver leg lengths. Another design modification was made to the small connecting links attached to the telescoping tubing (Figure 9, link r5). Originally, these links were designed to be fastened to the outside of the tubing (Figure 15). However, they were redesigned to provide greater stability by moving their attachment sites inward to the centerlines of the tubing (Figure 16).

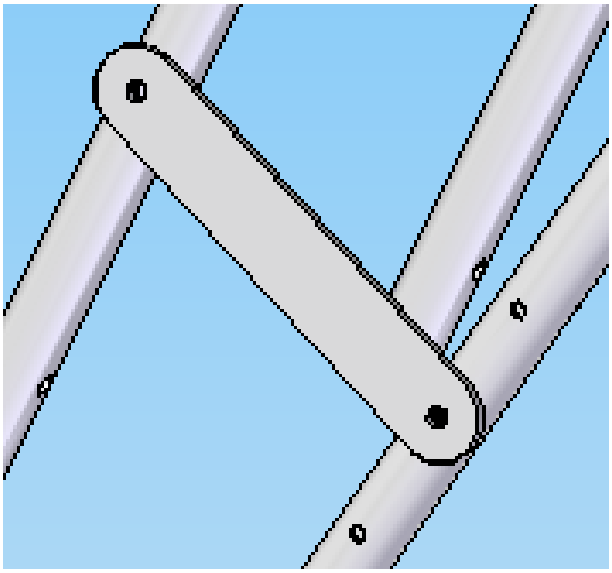

Figure 15: Initial connecting link design

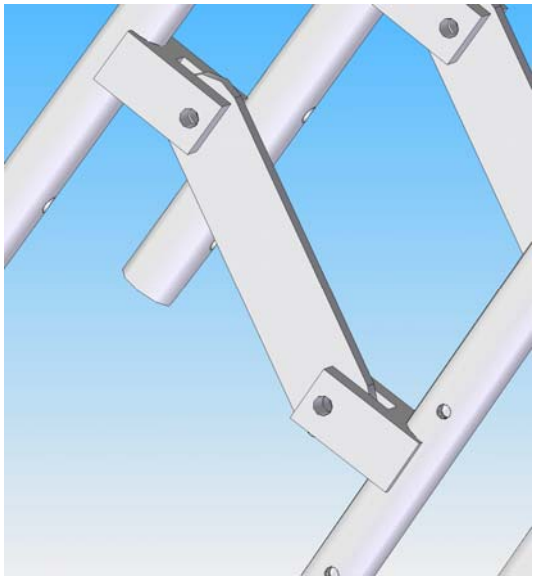

Figure 16: Final connecting link design

A second design change I made to the original mechanism was modifying the shape of the curved slider linkage (Figure 17). Accurately bending the aluminum tubing for this section of the device would have required sending the part to an outside machine shop, so in the interest of time and money I redesigned the section to be a rectangular shape composed of three separate sections of straight tubing (Figure 18).

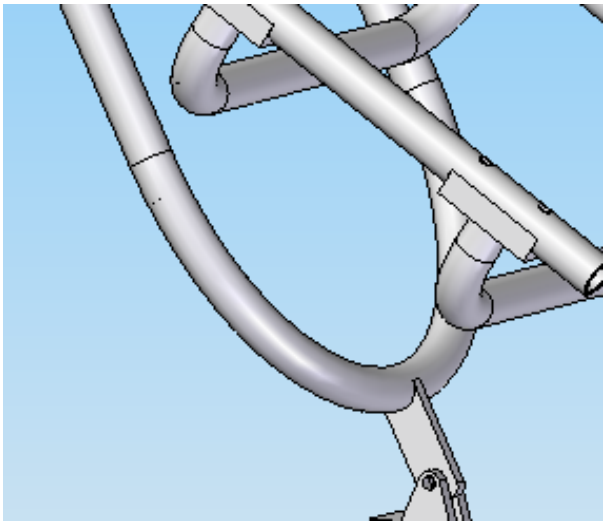

Figure 17: Initial slider linkage design

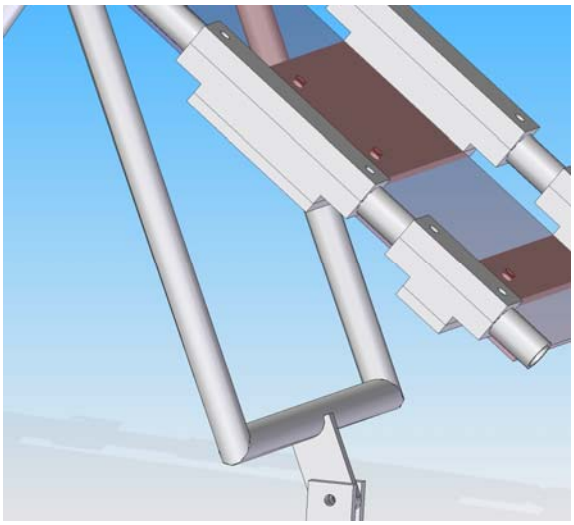

Figure 18: Final slider linkage design

Similarly, the crossbars spanning the tubing above the slider (Figure 19), were originally curved, but eventually modified for the final design. These crossbars are now flat sections of aluminum plate which also provide the mounting surface for the plate that supports the shank and foot of the cadaver specimen (Figure 20).

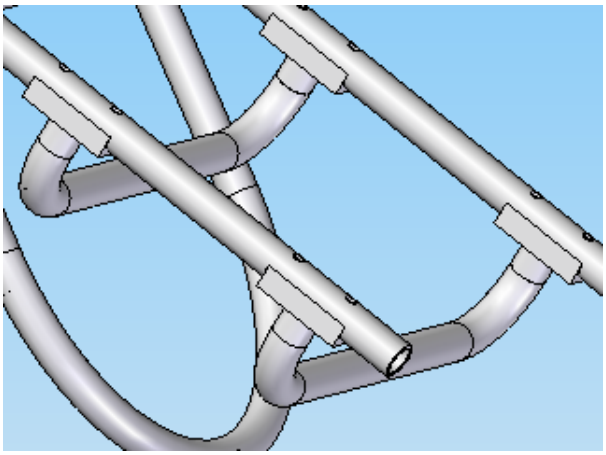

Figure 19: Initial crossbars design

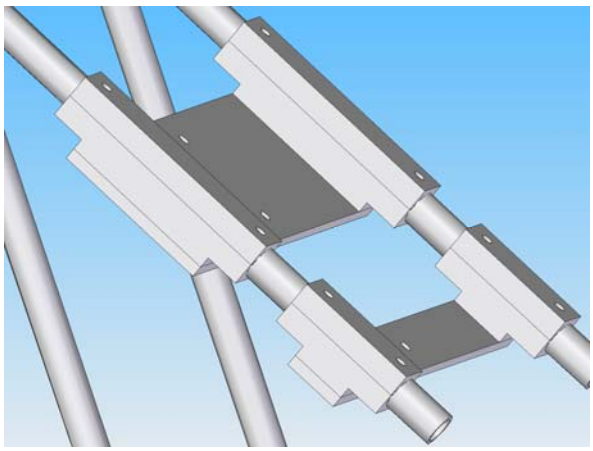

Figure 20: Final crossbars design

One of the biggest challenges for the final device was the design of the femur attachments. These parts of the mechanism must provide quick and simple attachment sites for various sizes of full cadaver legs as well as transected knees. Inserting long bolts through the bone and soft tissue of the thigh is a simple way to provide a rigid attachment of the femur, so I designed parts which are able to securely fasten these bolts to the frame. A set of blocks which attach to the top of the frame tubing provide holes through which the bolts can be inserted and fastened (Figure 21). These blocks provide an attachment site for bolts that are inserted horizontally through the sides of the cadaver leg specimen, which is ideal for avoiding interference with the soft tissue and muscles that are anterior and posterior to the femur. However, for transected knee specimens it may be easier to insert bolts through the top of the femur, requiring an attachment site on the frame below the specimen. To address this, I designed

crossbars similar to those underneath the shank and foot plate which are removable and provide an attachment site for vertical bolts (Figure 22).

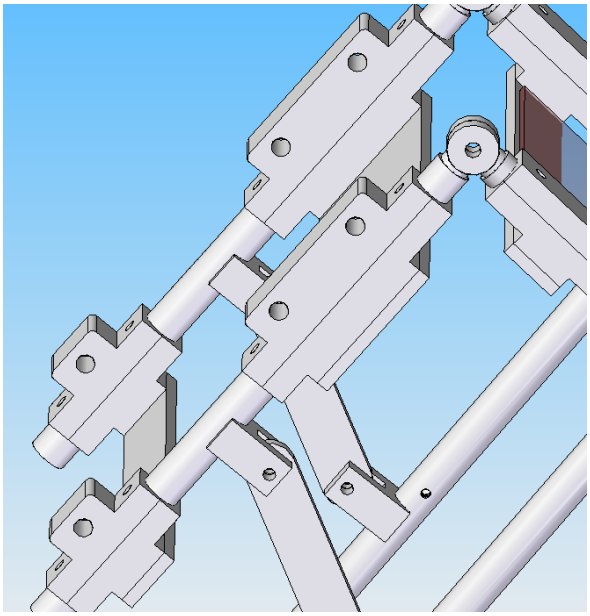

Figure 21: Horizontal Femur attachment blocks

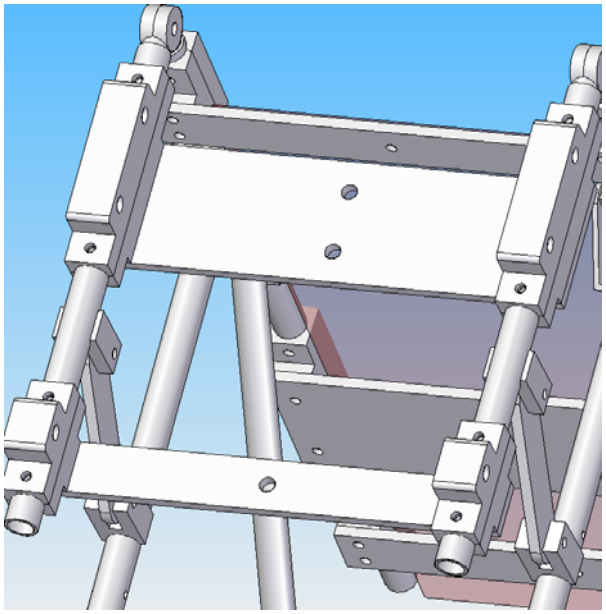

Figure 22: Vertical femur attachment crossbars

In designing these attachments I also had to consider how to ensure that the knee joint of the cadaver specimen would be in line with the rotating joint on the testing frame. The challenge was creating parts that would be adjustable for varying sizes of cadaver specimens. To solve this problem I designed spacers which could be inserted between the removable crossbar plates and the blocks which attach these plates to the underside of the frame tubing. In this way, the crossbars and femur attachments can be raised and lowered as necessary to accommodate varying specimen sizes and to maintain proper alignment of the knee joint.

After completing all of the necessary modifications, I created a model of the final design (Figure 23).

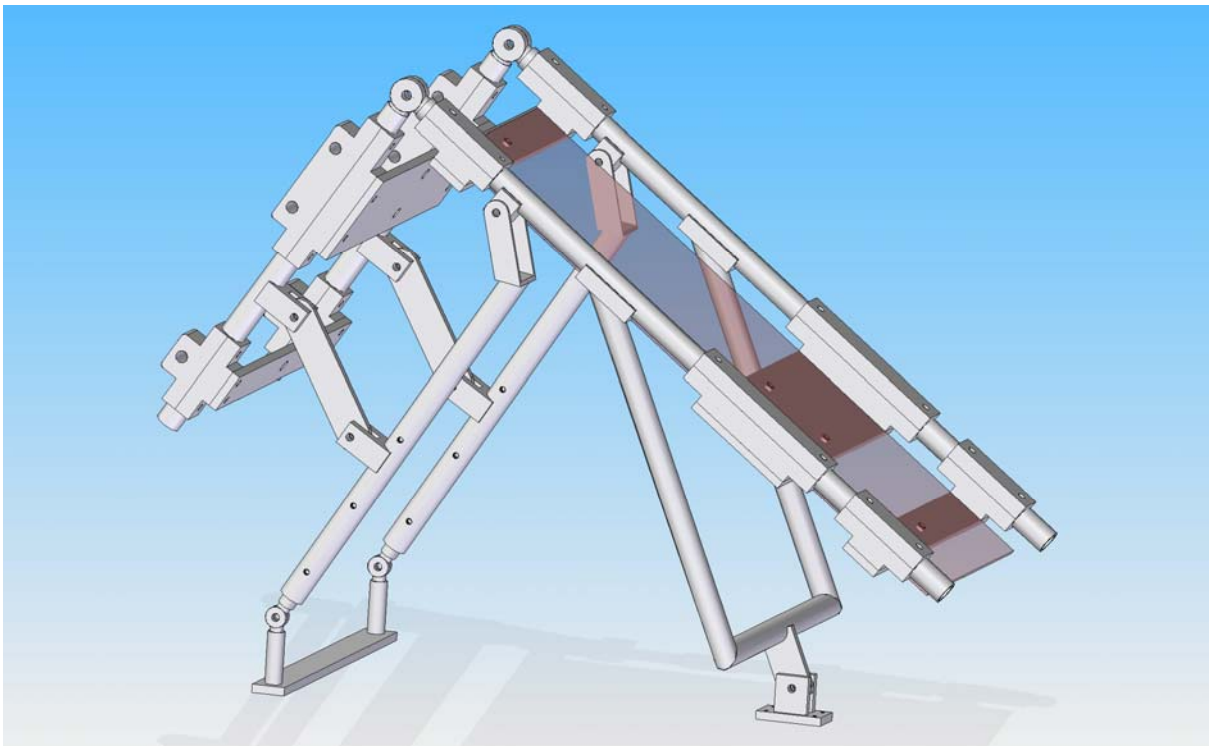

Figure 23: Final solid model
The final design is very similar to the initial design with a few important exceptions, including modifications to the connecting links, slider linkage, and crossbars as well as the addition of femur attachments.

The testing frame is made almost entirely of 6061-T6 aluminum, which was selected because of the material's light weight, good machinability, and low cost. The only non-metal part of the device is the plate which provides the support surface for the shank and foot of the cadaver leg specimen. To ensure that the six-degrees-of-freedom motion of the shank and foot are unconstrained, the plate material requires a very smooth surface. The plate is also designed to be removable to allow for easy cleaning, requiring a material which is both durable and lightweight. To meet these requirements, I selected a polycarbonate material called Lexan for the plate's construction.

Almost every individual part of the device, with the exception of the Lexan plate, was machined out of either aluminum tubing, plate, or extruded block. I machined every part myself in the Scott Laboratory student machine shop. The tubing, used almost exclusively for the links

of the testing frame, was roughly cut to size on either the vertical or horizontal band saw and then machined to their exact lengths using a Bridgeport milling machine. The holes in each section of tubing were also drilled with the milling machine. The machining process for the aluminum plate, used for the crossbars and a few smaller pieces in the frame, was very similar. Machining the aluminum blocks proved to be slightly more difficult. Most of the parts which attach to the tubing on either side of the cadaver specimen (including the femur attachments) are machined from these blocks. Additionally, I cut each of these parts out of a single aluminum piece using the horizontal band saw, which proved to be very time consuming due to the thickness of each block. I machined each of the blocks to their correct size using a shell cutter on the milling machine. The holes in each block were also made on the milling machine using various drill bits. To eliminate the rough edges which occurred as a result of using the band saws and milling machines, I used the belt sander on many of the finished parts.

The most difficult parts of the device to machine were the circular joints which connect the tubing on either side of the cadaver specimen and the joints which connect the telescoping tubing to the stationary base. After failing to find existing parts which could be used for these joints, I machined them from aluminum round bar that I found in the student machine shop. Each joint piece consists of a cylindrical shaft on one end which is press-fit into the end of the tubing and a flat circular section on the other end which forms the actual rotating joint. Each shaft was machined to size using the lathe in the machine shop. The flat circular joint section was then cut to size using the milling machine. To provide maximum stability to the testing frame, most of the non-removable parts were welded. All welding was completed by Gary Gardner in the Scott Laboratory machine shop. The machining and assembly of all of the individual components took approximately 3 months to complete (Figure 24).

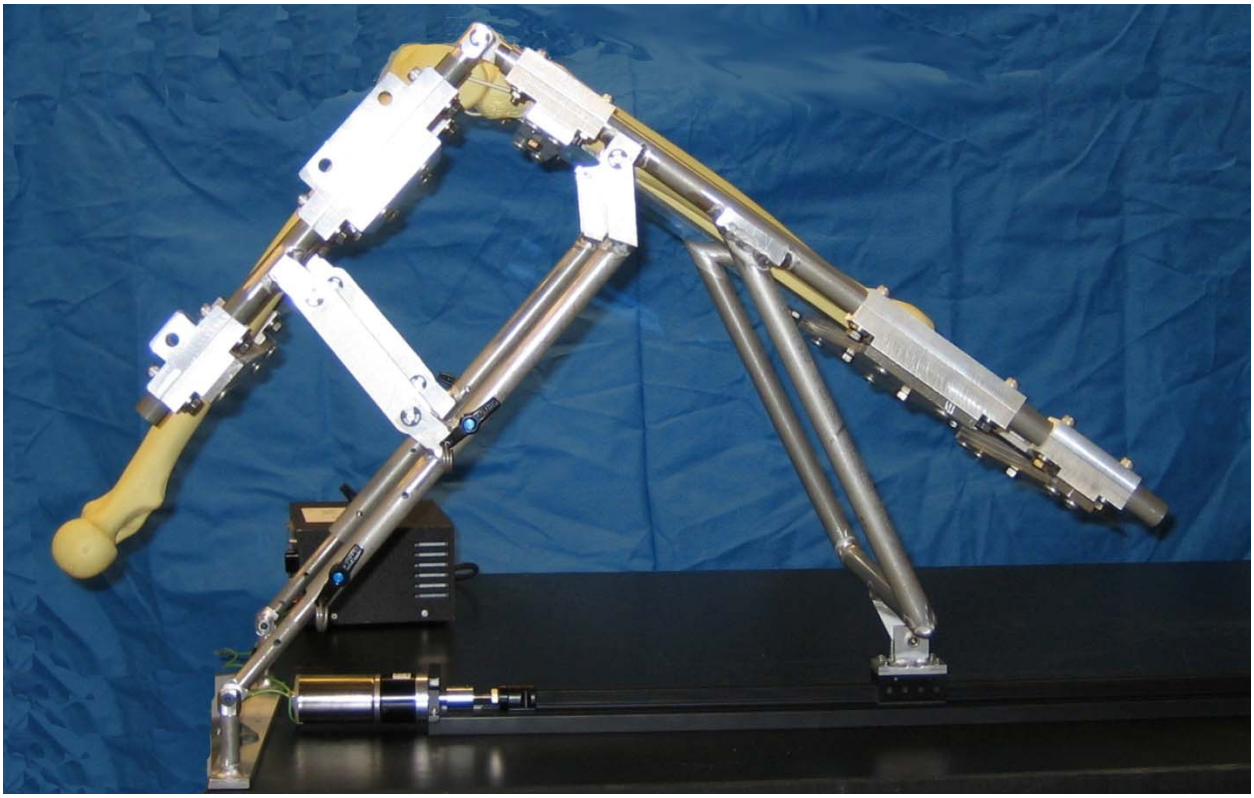

Figure 24: Final assembled device
Sawbones are attached to the device to represent the approximate position of the cadaver specimen. A motor is also connected to the shaft of the lead screw in the linear slide.

Chapter 4: Motion Control

To drive and control the lead screw in the linear slide requires a motor. I selected a DC motor for my application because of its good speed control capabilities, quiet operation, low maintenance, and reasonable price.

Based on the torque calculations from the linear slide analysis and the speed calculations from the vector loop analysis, I was able to calculate the minimum power requirement for the motor using the following equation:

$$\text{hp} = \frac{T * n}{63025}$$

Using the maximum calculated rotational speed of the screw:

$$\text{hp} = \frac{(1.459 \text{ in-lb})(953.15 \text{ rpm})}{63025} = 0.0221 \text{ hp}$$

The motor power in watts is:

$$0.0221 \text{ hp}\left(745.7 \ \frac{watts}{hp}\right) = 16.45 \text{ watts}$$

The motor speeds and move durations calculated from the linear velocity and position results for the slider will be used as input to control the motor. Currently, the motor is being controlled using open-loop feedback. We have run into some problems with using our LabVIEW and motion controller equipment, so for the time being we are varying motor speed by simply adjusting the voltage output on a power source. Eventually, we will be controlling the motor with closed-loop feedback through the use of a rotary potentiometer.

Chapter 5: Conclusion

The purpose of this project was to design, construct, and validate a cadaver knee motion testing device using passive motion for the purpose of understanding how surgical procedures affect knee kinematics.

5.1 Contributions

Knee surgeries are commonly used for the treatment of joint injury and disease. These surgeries affect knee joint kinematics. Understanding exactly how surgical procedures affect knee motion is required to be able to better restore knee function after surgery. Studying the motion of actual knees is ideal, however, since it is unethical to simulate surgery on living subjects there is a need for a device which utilizes cadaver specimens to simulate motion. The limitations of existing devices motivated the development of a new motion device.

Our custom passive motion device will allow us to investigate joint angles and speeds beyond the capabilities of existing devices. We will also be able to study the effects of rehabilitation protocols for various surgical procedures. This device has the added advantage of being able to simulate motion in both a full cadaver leg as well as a transected knee specimen. Using the calculations of position, speed, and force, we will be able to accurately control the motion of the device using a simple computer program. This custom passive motion device provides a versatile, accurate, simple, and cost-effective means for investigating many different procedures.

5.2 Additional Applications

The effects of a variety of procedures and surgical parameters on knee motion will be obtained using the device and will be beneficial in motivating possible future improvements in prosthetic design and surgical technique. Amongst the surgical procedures that can be investigated with this passive motion device are total knee arthroplasties (TKA's), ACL reconstruction, microfracture, and meniscal repair. The six-degree-of-freedom motion of the knee will be investigated at varying flexion angles and angular velocities. We will also be able to investigate the rehabilitation protocols after these surgeries and how rehabilitation is affected by angles and speeds that are outside the currently accepted ranges. In addition to studying the motion of the knee, we will also be able to study joint contact pressures between the bones of the knee, such as patellofemoral and tibiofemoral contact pressure.

Using this passive motion device, we can investigate the effects of varying prosthetic component alignment during TKA. We can study the affects of changing the placement of the patellar, tibial, and femoral prosthetic components on knee kinematics and contact pressure. In addition to investigating various alignments of the same prosthetic knee components, we can also

study the effects of different prosthetic designs, including posterior-stabilized, posterior cruciate-retaining and mobile-bearing designs.

5.3 Future Work

In addition to studying knee kinematics under passive loads, it is also important to study more realistic movements induced by simulated muscle forces. The study of active knee motion is necessary to understand how TKA affects normal activities of daily living, such as walking and stair climbing. The approach used in this project can be applied to the study of knee kinematics during active motion. Designing an active motion testing system will require finding a way to grab the muscles of the knee specimen so that simulated loads may be applied. These loads could be applied using various types of actuators, including motors and pneumatics.

Another useful tool for investigating active knee motion, especially during activities of daily living, is a dynamic computer simulation. Computer simulations can be used to address clinical questions such as how to improve patient functional outcome after knee surgeries such as TKA. While TKA provides excellent function for the low-demand everyday activities of older patients, there is a need to study how TKA can be adapted to allow more active patients to perform high-demand activities that are important to them. A previous study (Weiss et al., 2002) found that many patients value activities such as kneeling, gardening, squatting, and dancing, but most experience difficulty in performing these activities after knee replacement. Previous research (Piazza & Delp, 2001) has utilized forward dynamic computer simulations to predict knee motion during certain activities such as a step-up task, but no study has used a forward dynamic model to analyze the effect of altering component alignment on these functional tasks. Furthermore, as stated earlier, accurate modeling of joint contact surfaces, such as between the components of a total knee arthroplasty, is a challenging and computationally intensive step.

New algorithms are needed to reduce the computational time of contact modeling to make future patient-specific validation of intra-operative alignments feasible. I plan to use my knowledge of knee kinematics gained through my current project to develop a forward dynamic computer simulation that can predict postoperative outcome as a function of surgical parameters with the goal of improving individual patient outcome.

5.4 Summary

A custom passive motion device has been created which will allow us to investigate the effects of surgical procedures on the knee joint. This device has a number of advantages over existing devices, including range of speed capabilities, adaptability to many different sizes of cadaver specimens, a custom motion control system, and low cost. The design of the mechanism relied heavily on kinematic equations and a custom MATLAB program to determine position, speed, and force requirements. Machine design concepts were used to select the hardware and electronic components. The entire device was constructed in the mechanical engineering department's student machine shop. There are many possible applications for this device, including studies of knee surgeries and their effect on knee motion and contact pressures as well as studies of the effects of surgical parameters such as prosthetic component alignment in TKA. These studies will be beneficial in motivating possible future improvements in prosthetic design and surgical technique, thereby improving the function and quality of life of knee surgery patients.

Appendix A

MATLAB Code

```
%Position and velocity analysis with slider as input

r1=31.97;  %slider distance, inches

r_telescope=15.5; %telescoping link length, inches
r2=sqrt((r_telescope^2)+(2.125^2)-(2*r_telescope*2.125*cos(135*(pi/180))));

r3=16.461;
r4=0;
r5=4.875;
r6=7.6875;
r7=4.5625;
r8=8.45;
theta1=0;
theta4=0;

%Position
%slider-rocker:
A=-2*r1*r2*cos(theta1)-2*r2*r4*cos(theta4);
B=-2*r1*r2*sin(theta1)-2*r2*r4*sin(theta4);
C=r1^2+r2^2+r4^2-
r3^2+2*r1*r4*(cos(theta1)*cos(theta4)+sin(theta1)*sin(theta4));
t=(-B+sqrt(B^2-C^2+A^2))/(C-A);    %assembly mode +1

theta2=2*atan(t);
theta2degrees=(atan2(sin(theta2),cos(theta2)))*(180/pi);
beta1=(acos((r2^2+r_telescope^2-2.125^2)/(2*r2*r_telescope)))*(180/pi);

theta3=atan((r1*sin(theta1)+r4*sin(theta4)-
r2*sin(theta2))/(r1*cos(theta1)+r4*cos(theta4)-r2*cos(theta2)));
theta3degrees=(atan2(sin(theta3),cos(theta3)))*(180/pi);

%4-bar:
theta7=(theta3degrees+23.0214)*(pi/180);
theta7degrees=theta7*(180/pi);
theta8=(theta2degrees+10.241-beta1)*(pi/180);
theta8degrees=theta8*(180/pi);

A2=2*r7*r6*cos(theta7)-2*r8*r6*cos(theta8);
B2=2*r7*r6*sin(theta7)-2*r8*r6*sin(theta8);
C2=r7^2+r8^2+r6^2-r5^2-
2*r7*r8*(cos(theta7)*cos(theta8)+sin(theta7)*sin(theta8));

t2=(-B2-sqrt(B2^2-C2^2+A2^2))/(C2-A2);  %assembly mode -1
theta6=2*atan(t2);
theta6degrees=(atan2(sin(theta6),cos(theta6)))*(180/pi);
theta5=atan((r7*sin(theta7)+r6*sin(theta6)-
r8*sin(theta8))/(r7*cos(theta7)+r6*cos(theta6)-r8*cos(theta8)));
theta5degrees=(atan2(sin(theta5),cos(theta5)))*(180/pi);
```

```
alpha_degrees=theta7*(180/pi)-theta6degrees+180;
knee_flexion=180-alpha_degrees

%%
%Velocity
r1dot=41.511;  %slider velocity, inches/minute

%slider-rocker:
D=[-r2*sin(theta2) -r3*sin(theta3);r2*cos(theta2) r3*cos(theta3)];
E=[r1dot;0];
x=D\E;
theta2dot=x(1);
theta2dotdegrees=theta2dot*(180/pi);    %degrees/minute
theta3dot=x(2);
theta3dotdegrees=theta3dot*(180/pi);

%4-bar:
theta7dot=theta3dot;
theta8dot=theta2dot;

F=[-r5*sin(theta5) r6*sin(theta6);-r5*cos(theta5) r6*cos(theta6)];
G=[r8*theta8dot*sin(theta8)-
r7*theta7dot*sin(theta7);r8*theta8dot*cos(theta8)-r7*theta7dot*cos(theta7)];
y=F\G;
theta5dot=y(1);
theta5dotdegrees=theta5dot*(180/pi);
theta6dot=y(2);
theta6dotdegrees=theta6dot*(180/pi);

knee_flexion_speed=theta7dot*(180/pi)-theta6dotdegrees %speed in
degrees/minute

%%
%Static force analysis

F_thigh=100.085;    %force exerted by thigh, Newtons
F_shank=46.54;     %force exerted by shank
F_foot=14.512;      %force exerted by foot

com_thigh=9.352;    %center of mass position from knee, inches
com_shank=7.171;     %com position from knee
com_foot=18.413;     %com position from knee

F43_y=(-
F_thigh*com_thigh*cos(theta6))/(((r5*cos(abs(theta5))*r6*sin(theta6))/(r5*sin
(abs(theta5))))+(r6*cos(theta6)));
F43_x=-(F43_y*r5*cos(abs(theta5)))/(r5*sin(abs(theta5)));

F54_y=F_thigh+F43_y;
F54_x=F43_x;
F32_y=F43_y;
F32_x=F43_x;

r9=r_telescope;
```

```
r10=r9-6.8125;  %distance from telescoping revolute-ground joint to Link 2-3
joint
beta2=6.979;    %angle between link 5 and r3, degrees
alpha2=90-beta2-abs(theta3degrees);
a=12.875*sin(alpha2*(pi/180));
b=a/(cos(abs(theta7)));
c=(com_foot-8.5625)-b;
d=c*cos(abs(theta7));    %horizontal distance from foot force to slider
e=(8.5625-com_shank)*cos(abs(theta7));
f=e+a;      %horizontal distance from shank force to slider
g=(90-alpha2-11.915)*(pi/180);
beta4=(theta2degrees-5.089)*(pi/180);
beta5=beta4+(45*(pi/180));

h=(r10*F32_y*cos(beta4)-
r10*F32_x*sin(beta4))/(r9*cos(beta4)+2.125*cos(beta5));        %sum of
moments and forces equations used to find F52_x
i=-F_foot*d+F_shank*f-
h*16.461*cos(abs(theta3))+20.737*F54_y*cos(g)+20.737*F54_x*sin(g);
j=16.461*(sin(abs(theta3))+((cos(abs(theta3))*(r9*sin(beta4)+2.125*sin(beta5)
))/(r9*cos(beta4)+2.125*cos(beta5))));
F52_x=i/j;

F65_x=F52_x-F54_x;
F_slider=F65_x     %Horizontal force required at slider

%Passive motion position, speed, and force plots

x=[0 15 30 45 60 75 90 105 120];    %Knee flexion, degrees

%Minimum leg length

%Slider position
y1=[29.531 28.57 27.211 25.428 23.236 20.669 17.78 14.637 11.329];  %inches
p1=polyfit(x,y1,2);
a1=polyval(p1,x);

%Slider velocity
y2=[1.568 2.303 3.14 3.984 4.774 5.475 6.058 6.487 6.699];  %30 deg/min
angular velocity
p2=polyfit(x,y2,2);
a2=polyval(p2,x);
y3=[3.136 4.607 6.28 7.969 9.549 10.95 12.115 12.974 13.397];   %60
p3=polyfit(x,y3,2);
a3=polyval(p3,x);
y4=[4.705 6.91 9.42 11.953 14.323 16.425 18.173 19.462 20.096]; %90
p4=polyfit(x,y4,2);
a4=polyval(p4,x);
y5=[6.273 9.213 12.561 15.937 19.097 21.9 24.23 25.949 26.795]; %120
p5=polyfit(x,y5,2);
a5=polyval(p5,x);
y6=[7.841 11.516 15.701 19.922 23.872 27.375 30.288 32.436 33.493]; %150
p6=polyfit(x,y6,2);
a6=polyval(p6,x);
```

```
y7=[15.682 23.033 31.401 39.843 47.743 54.75 60.576 64.872 66.987]; %300
p7=polyfit(x,y7,2);
a7=polyval(p7,x);
y8=[25.523 34.549 47.102 59.765 71.615 82.126 90.864 97.308 100.48]; %450
p8=polyfit(x,y8,2);
a8=polyval(p8,x);
y9=[31.365 46.066 62.803 79.687 95.487 109.501 121.152 129.744 133.973]; %600
p9=polyfit(x,y9,2);
a9=polyval(p9,x);
y10=[39.206 57.582 78.503 99.608 119.359 136.876 151.44 162.181 167.466];
%750
p10=polyfit(x,y10,2);
a10=polyval(p10,x);

%Static force analysis
y11=[20.643 21.667 19.872 17.113 14.321 11.767 9.459 7.3 5.035]; %slider
force, lb

figure (1)
plot(x,y1,'xk')
grid on
hold on
plot(x,a1,'--k')
xlabel('Knee flexion angle (deg)')
ylabel('Slider distance from telescoping joint (inches)')
title('Slider Position')
legend('Position data','Best fit curve')

figure (2)
plot(x,y11,'-.xk')
grid on
xlabel('Knee flexion angle (deg)')
ylabel('Slider force (lbs)')
title('Static Force Analysis')

figure (3)
plot(x,y2,'+k',x,y3,'ok',x,y4,'*k',x,y5,'xk',x,y6,'sk')
grid on
hold on
plot(x,a2,'--k',x,a3,'--k',x,a4,'--k',x,a5,'--k',x,a6,'--k')
xlabel('Knee flexion angle (deg)')
ylabel('Slider speed (in/min)')
title('Slider Velocity (Commercial CPM)')
legend('30 deg/min','60 deg/min','90 deg/min','120 deg/min','150
deg/min','Best fit curve',2)

figure (4)
plot(x,y7,'ok',x,y8,'xk',x,y9,'+k',x,y10,'*k')
grid on
hold on
plot(x,a7,'--k',x,a8,'--k',x,a9,'--k',x,a10,'--k')
xlabel('Knee flexion angle (deg)')
ylabel('Slider speed (in/min)')
title('Slider Velocity (Experimental)')
legend('300 deg/min','450 deg/min','600 deg/min','750 deg/min','Best fit
curve',2)
```

```
%%
%Average Leg length

%Slider position
y1=[31.97 30.949 29.499 27.589 25.233 22.467 19.347 15.94 12.338];  %inches
p1=polyfit(x,y1,2);
a1=polyval(p1,x);

%Slider velocity
y2=[1.66 2.453 3.358 4.275 5.137 5.906 6.553 7.044 7.319];  %30 deg/min
angular velocity
p2=polyfit(x,y2,2);
a2=polyval(p2,x);
y3=[3.321 4.906 6.716 8.55 10.274 11.813 13.106 14.088 14.639];   %60
p3=polyfit(x,y3,2);
a3=polyval(p3,x);
y4=[4.981 7.359 10.074 12.825 15.411 17.719 19.659 21.132 21.958]; %90
p4=polyfit(x,y4,2);
a4=polyval(p4,x);
y5=[6.642 9.812 13.432 17.1 20.549 23.626 26.212 28.176 29.277]; %120
p5=polyfit(x,y5,2);
a5=polyval(p5,x);
y6=[8.302 12.265 16.79 21.375 25.686 29.532 32.766 35.221 36.596]; %150
p6=polyfit(x,y6,2);
a6=polyval(p6,x);

y7=[16.605 24.53 33.581 42.75 51.371 59.064 65.531 70.441 73.193]; %300
p7=polyfit(x,y7,2);
a7=polyval(p7,x);
y8=[24.907 36.795 50.371 64.125 77.057 88.597 98.297 105.662 109.789];  %450
p8=polyfit(x,y8,2);
a8=polyval(p8,x);
y9=[33.209 49.06 67.162 85.5 102.743 118.129 131.062 140.882 146.386]; %600
p9=polyfit(x,y9,2);
a9=polyval(p9,x);
y10=[41.511 61.325 83.952 106.875 128.429 147.661 163.828 176.103 182.982];
%750
p10=polyfit(x,y10,2);
a10=polyval(p10,x);

%Static force analysis
y11=[15.417 18.571 17.844 15.671 13.258 11.000 8.976 7.161 5.500]; %slider
force, lb

figure (5)
plot(x,y1,'xk')
grid on
hold on
plot(x,a1,'--k')
xlabel('Knee flexion angle (deg)')
ylabel('Slider distance from telescoping joint (inches)')
title('Slider Position')
legend('Position data','Best fit curve')

figure (6)
plot(x,y11,'-.xk')
```

```
grid on
xlabel('Knee flexion angle (deg)')
ylabel('Slider force (lbs)')
title('Static Force Analysis')

figure (7)
plot(x,y2,'+k',x,y3,'ok',x,y4,'*k',x,y5,'xk',x,y6,'sk')
grid on
hold on
plot(x,a2,'--k',x,a3,'--k',x,a4,'--k',x,a5,'--k',x,a6,'--k')
xlabel('Knee flexion angle (deg)')
ylabel('Slider speed (in/min)')
title('Slider Velocity (Commercial CPM)')
legend('30 deg/min','60 deg/min','90 deg/min','120 deg/min','150
deg/min','Best fit curve',2)

figure (8)
plot(x,y7,'ok',x,y8,'xk',x,y9,'+k',x,y10,'*k')
grid on
hold on
plot(x,a7,'--k',x,a8,'--k',x,a9,'--k',x,a10,'--k')
xlabel('Knee flexion angle (deg)')
ylabel('Slider speed (in/min)')
title('Slider Velocity (Experimental)')
legend('300 deg/min','450 deg/min','600 deg/min','750 deg/min','Best fit
curve',2)

%%
%Maximum Leg length

%Slider position
y1=[34.418 33.346 31.818 29.803 27.313 24.39 21.094 17.505 13.734];  %inches
p1=polyfit(x,y1,2);
a1=polyval(p1,x);

%Slider velocity
y2=[1.739 2.58 3.542 4.515 5.43 6.242 6.915 7.404 7.625];  %30 deg/min
angular velocity
p2=polyfit(x,y2,2);
a2=polyval(p2,x);
y3=[3.478 5.159 7.083 9.031 10.86 12.484 13.83 14.809 15.251];   %60
p3=polyfit(x,y3,2);
a3=polyval(p3,x);
y4=[5.217 7.739 10.625 13.546 16.291 18.725 20.744 22.213 22.876]; %90
p4=polyfit(x,y4,2);
a4=polyval(p4,x);
y5=[6.956 10.319 14.166 18.062 21.721 24.967 27.659 29.617 30.501]; %120
p5=polyfit(x,y5,2);
a5=polyval(p5,x);
y6=[8.695 12.899 17.708 22.577 27.151 31.209 34.574 37.022 38.127]; %150
p6=polyfit(x,y6,2);
a6=polyval(p6,x);

y7=[17.39 25.797 35.416 45.154 54.302 62.418 69.148 74.043 76.253]; %300
p7=polyfit(x,y7,2);
a7=polyval(p7,x);
```

```
y8=[26.085 38.696 53.124 67.731 81.453 93.627 103.721 111.065 114.38];  %450
p8=polyfit(x,y8,2);
a8=polyval(p8,x);
y9=[34.779 51.595 70.832 90.309 108.604 124.835 138.295 148.087 152.506];
%600
p9=polyfit(x,y9,2);
a9=polyval(p9,x);
y10=[43.474 64.493 88.54 112.886 135.755 156.044 172.869 185.109 190.633];
%750
p10=polyfit(x,y10,2);
a10=polyval(p10,x);

%Static force analysis
y11=[11.920 16.508 16.428 14.554 12.275 10.042 7.912 5.741 3.061]; %slider
force, lb

figure (9)
plot(x,y1,'xk')
grid on
hold on
plot(x,a1,'--k')
xlabel('Knee flexion angle (deg)')
ylabel('Slider distance from telescoping joint (inches)')
title('Slider Position')
legend('Position data','Best fit curve')

figure (10)
plot(x,y11,'-.xk')
grid on
xlabel('Knee flexion angle (deg)')
ylabel('Slider force (lbs)')
title('Static Force Analysis')

figure (11)
plot(x,y2,'+k',x,y3,'ok',x,y4,'*k',x,y5,'xk',x,y6,'sk')
grid on
hold on
plot(x,a2,'--k',x,a3,'--k',x,a4,'--k',x,a5,'--k',x,a6,'--k')
xlabel('Knee flexion angle (deg)')
ylabel('Slider speed (in/min)')
title('Slider Velocity (Commercial CPM)')
legend('30 deg/min','60 deg/min','90 deg/min','120 deg/min','150
deg/min','Best fit curve',2)

figure (12)
plot(x,y7,'ok',x,y8,'xk',x,y9,'+k',x,y10,'*k')
grid on
hold on
plot(x,a7,'--k',x,a8,'--k',x,a9,'--k',x,a10,'--k')
xlabel('Knee flexion angle (deg)')
ylabel('Slider speed (in/min)')
title('Slider Velocity (Experimental)')
legend('300 deg/min','450 deg/min','600 deg/min','750 deg/min','Best fit
curve',2)
```

Appendix B

Position, Speed, and Force Plots

Minimum Leg Length of 29.48”: telescoping link = 13”

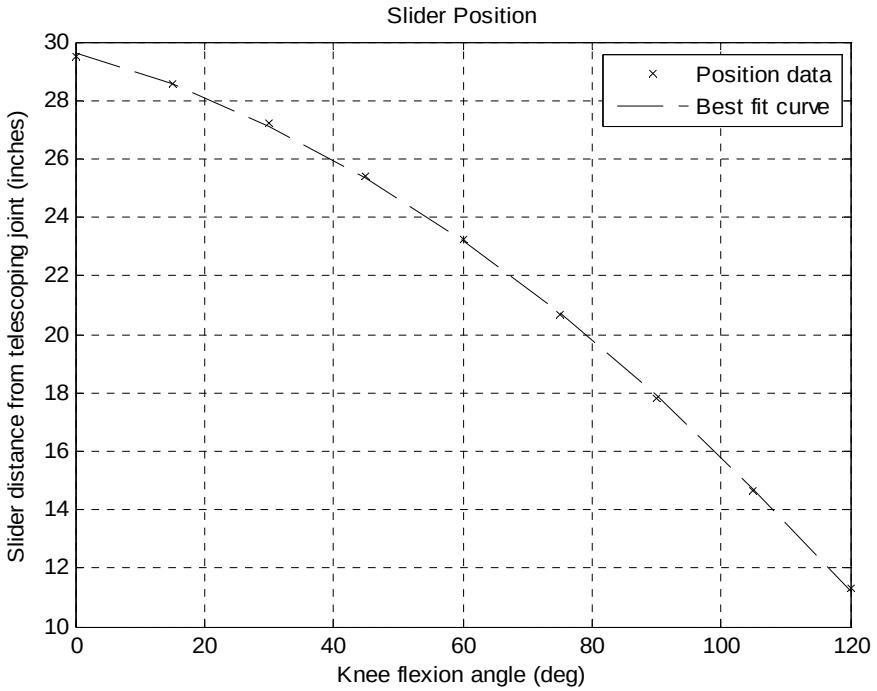

Figure 25: Plot of slider position vs. knee flexion angle (minimum leg length)

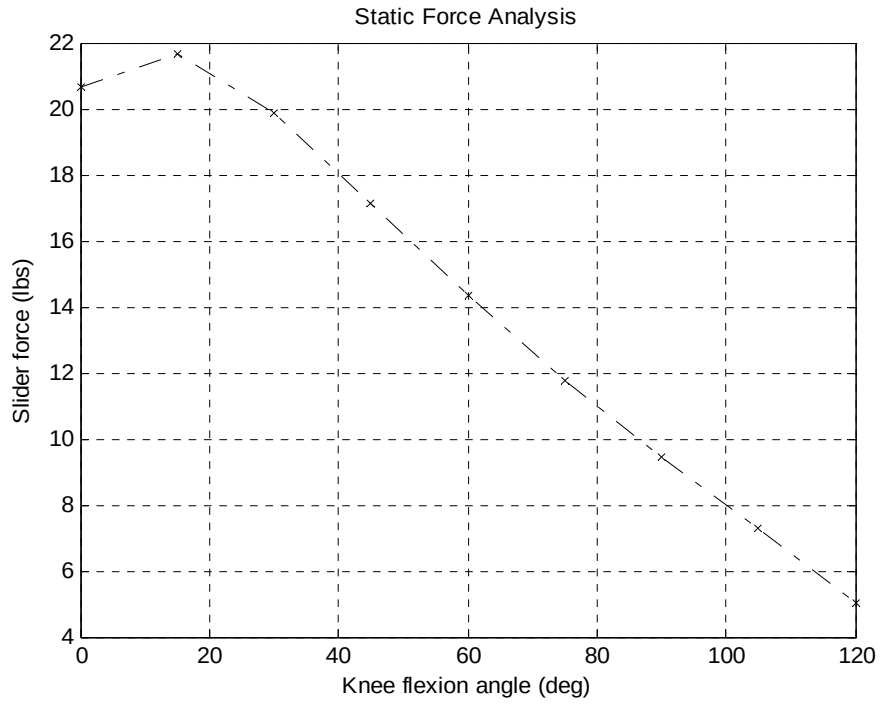

Figure 26: Plot of horizontal slider force vs. knee flexion angle (minimum leg length)

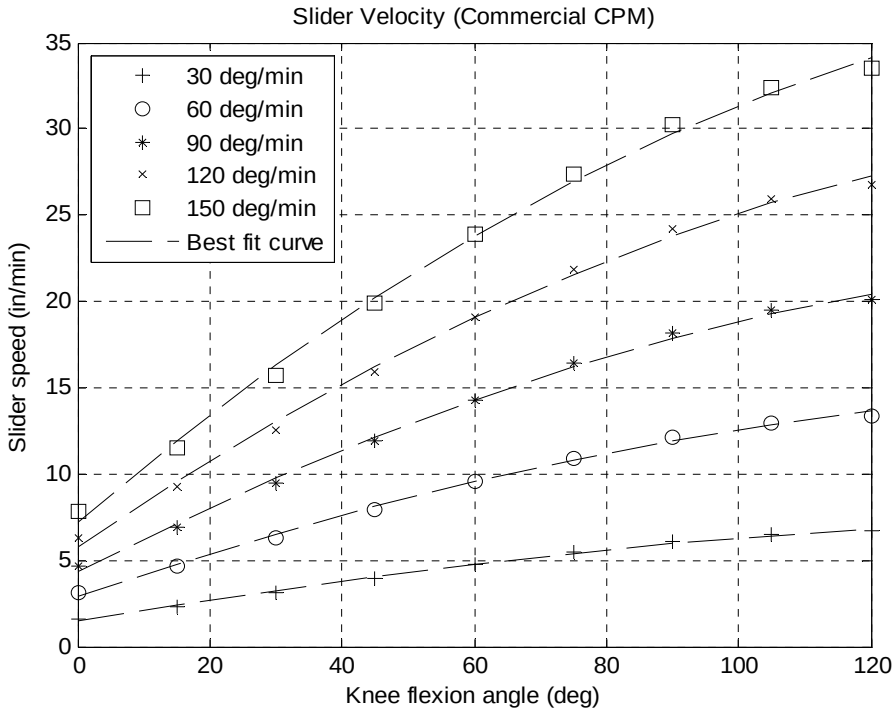

Figure 27: Plot of commercial CPM slider velocities vs. knee flexion angle (minimum leg length)

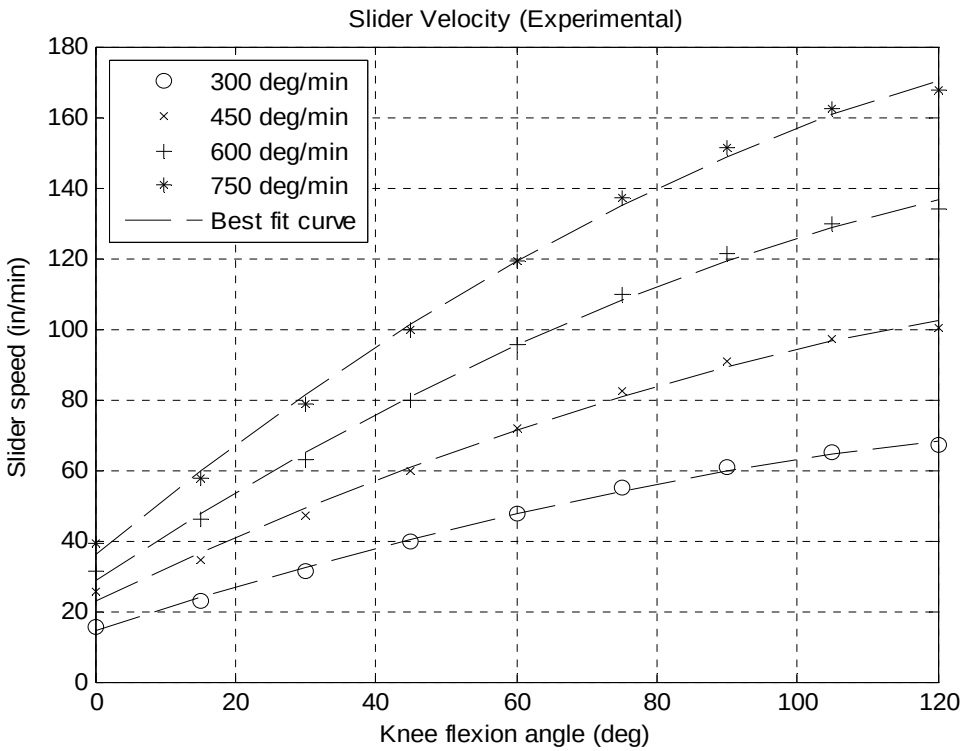

Figure 28: Plot of experimental slider velocities vs. knee flexion angle (minimum leg length)

Maximum Leg Length of 42.59”: telescoping link = 18”

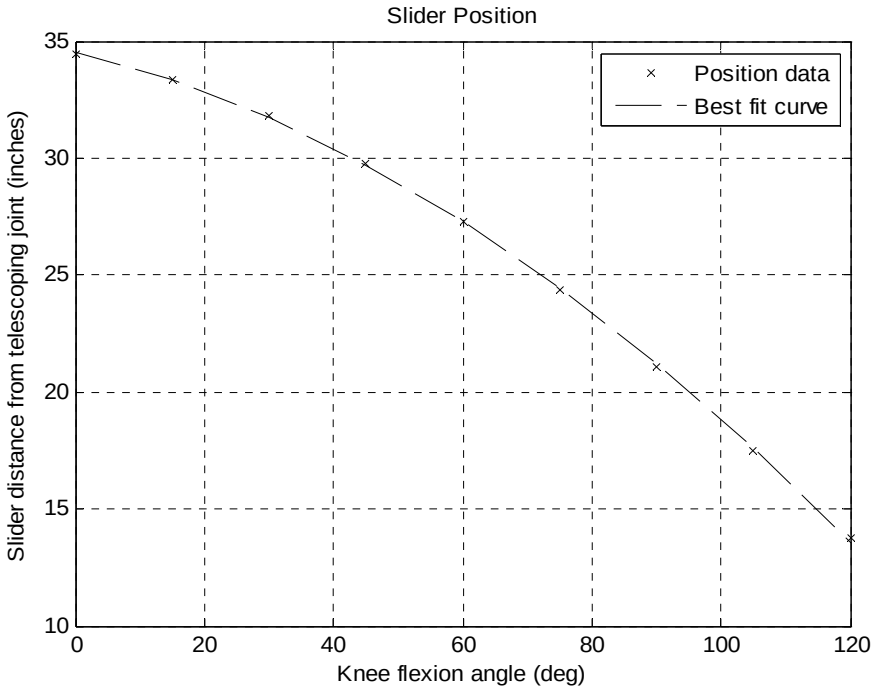

Figure 29: Plot of slider position vs. knee flexion angle (maximum leg length)

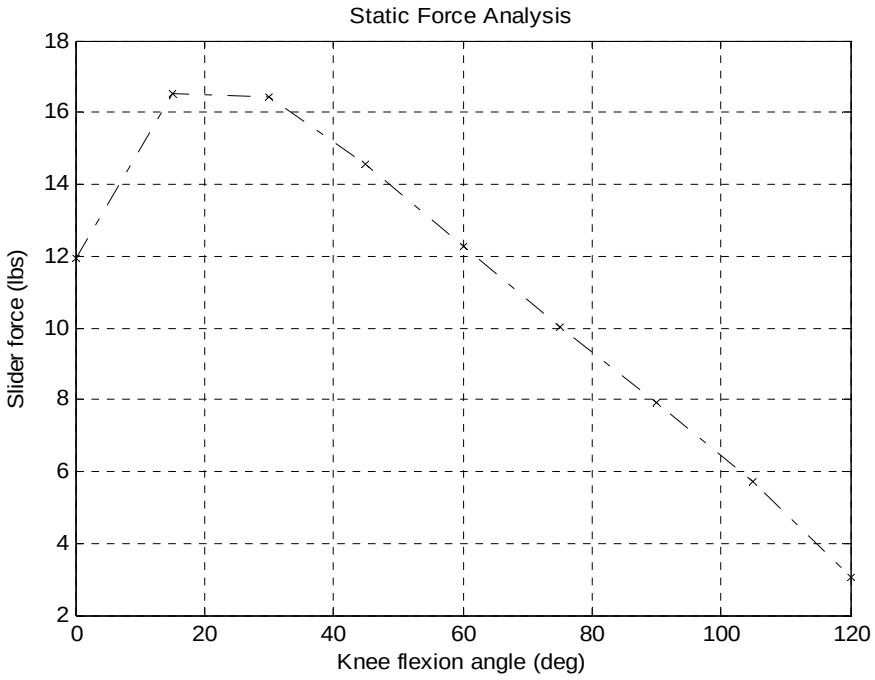

Figure 30: Plot of horizontal slider force vs. knee flexion angle (maximum leg length)

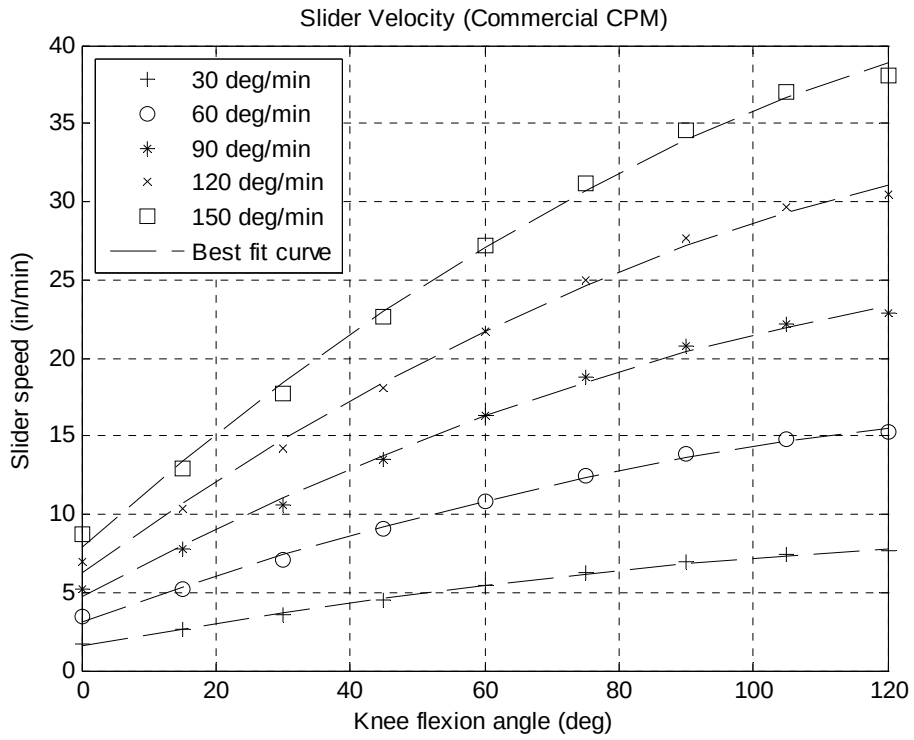

Figure 31: Plot of commercial CPM slider velocities vs. knee flexion angle (maximum leg length)

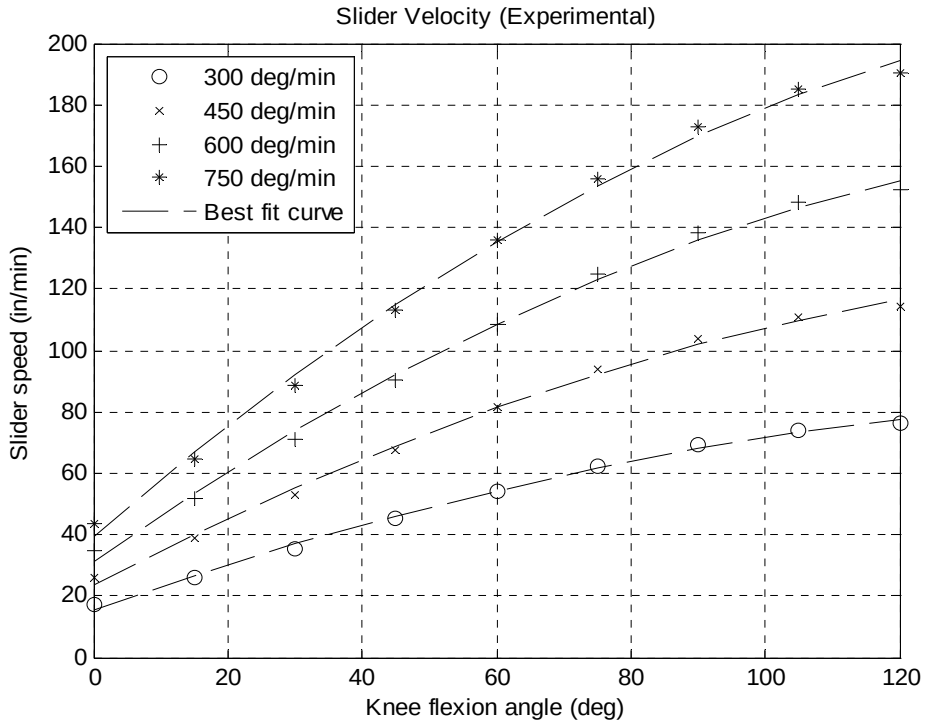

Figure 32: Plot of experimental slider velocities vs. knee flexion angle (maximum leg length)

Appendix C

Tables of Hardware and Electronics Comparisons

Table 5: Lead screw product comparison

Company	size	length	lead	material	part number	price	Comments
McMaster-Carr	3/8" - 10	36"	0.1	steel	98935A812	$11.86	2G (general) thread fit, Meets ASTM specs
Danaher motion	3/8" - 10	36"	0.1	stainless	SRA3710		0.01"/ft accuracy
Kerk motion products	3/8" - 10	36"	0.1		6010		53% efficiency

Table 6: Nut product comparison

Company	acme diameter	overall length	nut diameter	material	part number	price	comments
McMaster-Carr	3/8" - 10	0.62"	0.68"	bronze	95072A127	$22.40	round nut
McMaster-Carr	3/8" - 10	0.75"	1.35"	bronze	1343K133	$30.22	machinable round nut
Danaher Motion	3/8" - 10			bronze	BN3710		38% efficiency
Kerk motion products	3/8" - 10	1.0"	0.63"		BF6000		Flange: thickness=0.19, dia=1.13

Table 7: Screw and nut assembly product comparison

Company	size	length	lead	screw material	nut material	part number	price	Lead time
Nook Industries	3/8"	36"	0.1	steel	bronze	030-RA/EK/CN/36/20030/FS	$1,063.32	3 weeks

Table 8: Linear slide product comparison

Company	Screw Dia.	Lead	Screw material	Nut material	Torque to move load	Design Load	Part Number	Price	Comments
Kerk Motion Products	3/8"	0.1	stainless	plastic	1 oz-in/lb	35 lbs	RGS6010T X 36"	$ 286.20	Lead is too small for speeds we want to use
Kerk Motion Products	3/8"	0.5	stainless	plastic	2.5 oz-in/lb	35 lbs	RGS6050T X 36"	$ 286.20	Angular control is not ideal
Kerk Motion Products	3/8"	0.5	stainless	plastic	2.5 oz-in/lb	35 lbs	RGSWX6050T X 36"	$ 493.50	Includes a motor mounting plate for a NEMA 17 motor (motor not included)
Kerk Motion Products	3/8"	0.2	stainless	plastic	1.5 oz-in/lb	35 lbs	RGSWX6020T X 36"	$ 493.50	Sufficient lead for experimental speeds and good angular control
Intelligent Motion Systems	3/8"	0.1	stainless		1 oz-in/lb	35 lbs	MDM1PSD17B4-RA36	$ 614.00	Includes a Mdrive 17x2 stack motor
							MD-CC300-000	$ 98.00	configuration cable
Intelligent Motion Systems	3/8"	1	stainless		4.5 oz-in/lb	35 lbs	MDMPSD23C7-RD36	$1,049.00	Includes a NEMA 23x3 stack microstepping Mdrive motor.
							IP804	$ 153.89	Power Supply, 75V output
Lintech Motion	16 x 16 NPL ball screw	16 mm	case hardened steel				104430-CP0-1-S120-M02-C000-L00-E00-B00	$2,305.00	max speed=18 in/sec. Includes NEMA 23 motor mount.

Table 9: Motor product comparison

Company	Rated Voltage	Rated Speed (RPM)	Rated Power	Peak Torque	Continuous Stall Torque	Length	Part Number	Price	Comment
Anaheim Automation	36V	4000	95 W	100 oz-in		3.8"	BLWR23MD3S-36V-4000	$ 177.00	integrated motor/driver
Anaheim Automation	24V	4000	110 W	106 oz-in	42 oz-in	3.9"	BLY174S-24V-4000	$ 71.00	brushless DC motor
Anaheim Automation							MDC150-050301	$ 129.00	brushless DC driver
Bodine Electric Co		10000	1/5 hp		20 oz-in	4.63"	3314	$ 266.00	
Bodine Electric Co		10000	1/3 hp		33 oz-in	4.56	3317	$ 328.00	
Danaher Motion	48V	10000	121 W	4.2 lb-in	1.9 lb-in	4.25"	PMB11D		
Danaher Motion	75V	8000	111W	5.4 lb-in	1.64 lb-in	2.74"	AKM11E		
Motor Technology Inc.	12V	9140	0.1 hp	14 oz-in	183 oz-in		230A100-1	$1,430.50	military quality

References

Andriacchi, T.P., Alexander, E.J., Toney, M.K., Dyrby, C. and Sum, J., 1998. A point cluster method for in vivo motion analysis: applied to a study of knee kinematics. Journal of Biomechanical Engineering 120, 743-749.

Andriacchi, T.P., Dyrby, C.O., Johnson, T.S., 2003. The use of functional analysis in evaluating knee kinematics. Clinical Orthopaedics and Related Research 410, 44-53.

ACL Solutions, 2001. Anatomy of the Knee. Medical Internet Solutions, L.L.C.. http://www.aclsolutions.com/anatomy.php.

Balasubramanian, S., Demetropoulos, C. K., Bilkhu, S. K., & Yang, K. H., 2007. Force Couple Testing System - A New Method for Measuring the *In Vitro* Knee Kinematics. 53rd Annual Meeting of the Orthopaedic Research Society. Poster No. 0774.

Banks, S.A., Hodge, W.A., 2004. Implant design affects knee arthroplasty kinematics during stair-stepping. Clinical Orthopaedics and Related Research 426, 187-193.

Collins, J. A., 2003. Mechanical Design of Machine Elements and Machines. John Wiley & Sons, Inc.

eOrthopod, 2002. Anterior Cruciate Ligament Injuries. Medical MultiMedia Group, LLC., www.eorthopod.com.

Kerk Motion, 2008. RGS and RGSW Linear Slides. Kerk Motion Products, Inc., www.kerkmotion.com.

Knee., 2007. In *Wikipedia* [Web]. Wikimedia Foundation, Inc.. from http://en.wikipedia.org/wiki/Knee.

Li, G., Zayontz, S., DeFrate, L. E., Most, E., Suggs, J. F., & Rubash, H. E., 2004. Kinematics of the knee at high flexion angles: an in vitro investigation. Journal of Orthopaedic Research 22, 90-95.

O'Driscoll, S.W., Giori, N.J., 2000. Continuous passive motion (CPM): Theory and principles of clinical application. Journal of Rehabilitation Research and Development 37 (2), 179-188.

Piazza, S.J., Delp, S.L., 2001. Three-dimensional dynamic simulation of total knee replacement motion during a step-up task. Journal of Biomechanical Engineering 132: 599-606.

Piazza, S.J. 2006. Muscle-driven forward dynamic simulation for the study of normal and pathological gait. Journal of NeuroEngineering and Rehabilitation 3:5: 1-7.

Shiel, W. C., 2006. Osteoarthritis (Degenerative Arthritis). MedicineNet.com Web site: http://www.medicinenet.com/osteoarthritis/article.htm.

Siston, R.A., Giori, N.J., Goodman, S.B., Delp, S.L., 2006. Intraoperative passive kinematics of osteoarthritic knees before and after total knee arthroplasty. Journal of Orthopaedic Research 24, 1607-1614.

Waldron, K. J., Kinzel, G. L., 2004. Kinematics, Dynamics, and Design of Machinery, 2nd ed. John Wiley & Sons, Inc.

Weiss, J. M., Noble, P. C., Conditt, M. A., Kohl, H. W., Roberts, S., Cook, K. F., Gordon, M. J., & Mathis, K. B. (2002). What functional activities are important to patients with knee replacements?. *Clinical Orthopaedics and Related Research. 404*, 172-188.

Wilson, D. R., Feikes, J. D., Zavatsky, A. B., & O'Connor, J. J., 2000. The components of passive knee movement are coupled to flexion angle. Journal of Biomechanics *33*, 465-473.

Winter, D. A., 2005. Biomechanics and motor control of human movement. 3rd edition. John Wiley & Sons.

Zimmer, 2006. Osteoarthritis. Zimmer, Inc., www.zimmer.com.